Dear reviewer,

We appreciate that you provided the valuable comments for the improvement of the manuscript. Following your thoughtful suggestions, we have revised the manuscript very carefully. The lists below are the responses to each comment.

General comments

The authors have provided a potential novel methodology to estimate total suspended solids concentrations of estuaries and coastal areas of China. However, we have a number of concerns about the approach that should be considered before being allowed to advance further through the review process. Unfortunately, there are numerous grammatical and structural errors throughout the document which has made comprehension difficult in some places. The flow between sentences, and paragraphs could be improved, with better linkages between ideas, concepts and explanations. Before the next submission, we strongly suggest having a native English speaker review and correct the manuscript.

Response:

Thanks a lot for the valuable comments about the grammatical and structural issues. Following your suggestions, we have asked for **native speakers** (two associated professors of USA) helping us to pick up grammatical errors and revise the manuscript very carefully. **In addition**, reviewer #1 had also helped to point out main writing errors and structural issues and revised our manuscript carefully. Now the linkage of sentences, paragraphs had been polished and added in many places for the improvement of flow, structure and readability of the manuscript, which is helpful to outline the general modelling strategy more clearly (Page 3, line 19; Page 15, line 14; Page 6, lines 21-25; Page 9, lines 2-4; Section 2.1; Section 2.4; Section 2.5; Section 3.4). The contents of "extraction of water bodies" in Section 3.4 is removed to Section 2.1 (Page 6). The contents of the "Band response function application of Landsat sensors for field spectra" in Section 3.1 have been moved to Section 2.4 (Page 10). All the revising have been marked in red in the marked-up mode (Page 1, lines 1-2, 14-15, 17-23, 25-28; Page 2, lines 1-2, 5-6, 10; Page 3, lines 1-4, 15-16, 18-19, 26; Page 4, lines 20-22, 24-27; Page 5, lines 9-10, 17-18, 22-23; Page 6, lines 5-6, 13-14, 21-25; Page 7; Page 8, lines 1-6, 10-15, 17, 22, 26-27; Page 9, lines 1-3, 7-9, 12-15, 18-21; Page 10, lines 10-11, 14-16; Page 11, lines 6-7; Page 12, lines 2-4; Page 13, lines 14-21, 24; Page 14, lines 18-19; Page 15, lines 6-9, 19-22; Page 16, lines 4-9, 16, 26-27; Page 17, lines 6-7, 17-20, 23-24; Page 18, lines 4-5, 14, 19-23, 27; Page 19, lines 1-4, 6, 9-10, 17, 21-23). We expect that the revised manuscript will meet the demand of Journal.

While the background is quite easy to follow, the rationale for this study and what it is aiming to achieve could be better articulated. It is not clear in the abstract that the authors are evaluating a model they themselves have developed nor does it mention the novelty of their approach. It reads more like they are just testing an existing method. They also mention the 'adjusted' QRLTSS model (line 18), but I am not sure how this differs to the QRLTSS model mentioned in the previous sentence (line 16).

Response:

We are very sorry that there are controversial words and imprecise statements confusing the understanding of the text. This study did NOT test an existing method. Based on 119 in-situ samples collected in 2006-2013 from five regions of China, this study **developed** the QRLTSS model by **reviewing** a number of Landsat-based TSS retrieval models and **improving** a relatively better one among them. About the "adjusted", we meant improving before. The QRLTSS model mentioned in the manuscript is all the **same one**. We have revised the statements in whole manuscript very carefully to avoid the confusion correspondingly. (Page 1, lines 18-19, 25; Page 2, lines 1-2, 5, 10; Page 12, line 3; Page 18, lines 19, 21, 23, 27; Page 19, lines 6, 10, 17).

Of particular concern is the sampling method for the in-situ data. There is a lack of information about the time and depth of each sample, and then how this corresponds to the timing of the satellite image used in the analysis. Samples were taken between 10 am to 5 pm, during which it is likely tides may have significantly altered turbidity and TSS concentrations. But the tidal effect on turbidity has not been mentioned. Further some analysis of the time of the satellite image and the sample should be undertaken – a longer length of time between the two may impact the accuracy of results.

Response:

There was a mistake to summarize the information of sampling succinctly in **previous version**. However, we still showed some necessary information about in-situ samples. The water samples and synchronous field spectral measurements were carried out from **10:00 to 15:00** (Page 7, lines 8-9) **rather than 10:00 to 5 pm**. The spectrum were measured based on above-water spectrum measurement method (Tang et al., 2004) (Page 7, lines 12-13). Water samples (about 1.5 L) were collected within the water depth of 1 m. TSS concentrations were measured from water samples by a weighed method (Binding et al., 2012; Caballero et al., 2014) (Page 7, lines 18-19). The sampling method for the in-situ data followed the community accepted standards and was applied widely (Chen et al., 2015; Feng et al., 2014; Zhang et al., 2014) (Page 7, lines 13-14). So, the samples are not difficult to correspond to the timing of the satellite image used in the study.

Following your suggestions, we have revised the relevant statements to make it clearer (Page 7, lines 8-19).

It is right that a longer length of time between sample and satellite image may impact the accuracy of results. Thus, we selected the samples within **two-hour time** window of satellite overpass to validate the accuracy of the QRLTSS model similar to the previous studies (Bailey and Werdell. 2006; Chen et al., 2015; Zhang et al., 2014) (Page 15, lines 16-18; Page 17, lines 25-27).

Indeed, tides would significantly altered turbidity and TSS concentrations as you pointed out. However, the samples were taken mainly from 10:00 to 15:00 (Beijing time) (Page 7, lines 8-9) and the samples used for validation were within **two-hour time** window of satellite overpass in the study (Page 15, lines 16-18; Page 17, lines 25-27). Thus, the tidal effect on turbidity is relatively small (Bailey and Werdell. 2006; Chen et al., 2015). In addition, we had simply analyzed the spatial variation of TSS concentrations with the impact of interaction of tide and runoff in the manuscript (Page 16, lines 10-12, 17-18; Page 17, lines 7-8). The tidal effect on turbidity you pointed out is an interesting question and deserves the further study.

References:

Bailey, S.W., & Werdell, P.J.: A multi-sensor approach for the on-orbit validation of ocean color satellite data products. Remote Sensing of Environment, 102, 12-23, doi.org/10.1016/j.rse.2006.01.015, 2006.

Binding, C.E., Greenberg, T.A., & Bukata, R.P.: An Analysis of MODIS-Derived Algal and Mineral Turbidity in Lake Erie. Journal of Great Lakes Research, 38, 107-116, doi.org/10.1016/j.jglr.2011.12.003, 2012.

Caballero, I., Morris, E.P., Ruiz, J., & Navarro, G.: Assessment of suspended solids in the Guadalquivir estuary using new DEIMOS-1 medium spatial resolution imagery. Remote Sensing of Environment, 146, 148–158, doi.org/10.1016/j.rse.2013.08.047, 2014.

Chen, J., Quan, W., Cui, T., & Song, Q.: Estimation of total suspended matter concentration from MODIS data using a neural network model in the China eastern coastal zone. Estuarine, Coastal and Shelf Science, 155, 104-113, doi.org/10.1016/j.ecss.2015.01.018, 2015.

Feng, L., Hu, C., Chen, X., & Song, Q.: Influence of the Three Gorges Dam on total suspended matters in the Yangtze Estuary and its adjacent coastal waters: Observations from MODIS. Remote Sensing of Environment, 140, 779–788, doi.org/10.1016/j.rse.2013.10.002, 2014.

Tang, J., Tian, G., Wang, X., Wang, X., & Song, Q.: The Methods of Water Spectra Measurement and Analysis: Above-Water Method. Journal of Remote Sensing, 8, 37-44, 2004.

Zhang, M., Dong, Q., Cui, T., Xue, C., & Zhang, S.: Suspended sediment monitoring and assessment for Yellow River estuary from Landsat TM and ETM+ imagery. Remote Sensing of Environment, 146, 136–147, doi.org/10.1016/j.rse.2013.09.033, 2014.

Finally, we would like some justification for the location of the samples taken. Sampling locations tend to be in areas which have similar turbidity characteristics and do not represent the wide variability of tss/turbidity within the individual estuaries and coastal areas under investigation. As a result, we have concerns about the validity of the approach for extrapolating over larger areas in which there will be a large amount of variability in TSS concentrations. We would recommend that the limitations of the work are discussed more thoroughly with this in mind. Alternatively, considerably more samples would need to be collected that cover a wider area of the estuaries and coastal areas under investigation.

Response:

In-situ samples, covering wide ranging of turbidity, are important to the calibration and variation of TSS model in estuaries and coasts.

In our study areas, Xuwen coast is **a less turbid region** due to less water discharge, sediment load and protection of coral reef (Page 5, lines 7-10). The mean distance of two samples is more than 0.8 km and the farthest distance is about 23.98 km (Page 31, figure 1b), which covers a large area of Xuwen coast (10.77%), including two core areas and a buffer area in Xuwen Coral Reef Reserve. TSS concentrations of the 32 samples ranges from **4.3 mg/L** to **37.8 mg/L** with a mean value of **11.2 mg/L** in Xuwen coast. These samples represent the variability of TSS concentrations in the region well.

TSS concentrations in Moyangjiang River Estuary, Pearl River Estuary and Hanjiang River Estuary of Guangdong Province (Page 31, figure 1c, d, e) were mainly affected by the interaction of runoff and tide. So, the samples in the three estuaries (Page 31, figure 1c, d, e) with the **almost same representativeness** were carried out from the **lower river reaches** to the **outer shelf area (**including shoals, channels, maximum turbidity zones). TSS concentrations of the total of 62 simples (Page 31, figure 1c, d, e) in the three estuaries ranging from **5.2 mg/L** to **220.7 mg/L**. Among them, TSS concentrations of 15 simples ranges from 106 mg/L to 220.7 mg/L with a mean value of **150.9 mg/L**. In addition, the mean distance of two samples and the farthest distance from lower river reaches in the three estuaries are more than 0.7 km and about **15.3 km** in Moyangjiang River Estuary (Page 31, figure 1c), 1.3 km and **27.4 km** in Pearl River Estuary (Page 31, figure 1d) and 0.7 km and **8.7 km** in Hanjiang River Estuary (Page 31, figure 1e), respectively. We believe that the samples can reflect the characteristic of turbidity of estuaries of Guangdong Province well.

Besides, TSS concentrations of the 34 samples in Yangtze Estuary (Page 31, figure 1f) ranges from **38.4 mg/L** to **577.2 mg/L** with a mean value of 178.2 mg/L. The mean distance of two samples is more than **2.6 km** and the farthest distance from lower river reaches is about **73.32 km** (Page 31, figure 1f). These samples reflect the large variation of TSS concentrations of Yangtze River well.

We also agree that the more samples could represent the high-dynamic TSS concentrations in larger areas better. However, in-situ data collection is very difficult plus the budget issue and weather during the satellite overpass, especially in coastal oceans of cloudy and rainy south China. We collected the samples funded by several projects for many years. Now, we have added the statements to present the representativeness of the location or concentrations of the samples clearer (Pages 7, lines 1-4).

Specific comments

Abstract – states 129 samples were used but in the body of the text 119 were used in total.

Response:

Sorry for the confusing statement. In fact, there are **129** in-situ samples in total collected from the study areas (Page 6, line 27). Among them, there are **119** in-situ samples with field spectral measurements and synchronous water samples (TSS concentrations) (Page 7, lines 8-9. Table 1). **Another ten** in-situ samples **have TSS concentration only** (Page 7, lines 9-11. Table 1). So, the **119** in-situ samples were used to calibrate (N=84) and validate (N=35) the QRLTSS model respectively. The other **ten** in-situ samples of TSS were **only** used to **further validate** the accuracy of the QRLTSS model from remote sensing inversion of Hyperion image. We have revised the statement to make it clearer (Page 1, line 17).

Page 7, line 7-10. Please explain ETM+, TM and OLI in more detail and how they differ.

Response:

The Landsat Thematic Mapper (**TM**) sensor was carried on Landsat 4 and Landsat 5, and images consist of six spectral bands with a spatial resolution of 30 meters for Bands 1-5 and 7 (**Band 1 -** Blue, 0.45 - 0.52 µm; **Band 2 -** Green, 0.52 - 0.60 µm; **Band 3 -** Red, 0.63 - 0.69 µm; **Band 4 -** Near Infrared, 0.76 - 0.90 µm; **Band 5 -** Shortwave Infrared (SWIR 1), 1.55 - 1.75 µm and **Band 7 -** Shortwave Infrared (SWIR 2), 2.08 - 2.35 µm) and one thermal band (**Band 6** – Thermal, 10.40 - 12.50 µm) (https://landsat.usgs.gov/).

The Landsat Enhanced Thematic Mapper Plus (**ETM+**) sensor is carried on Landsat 7, the seventh satellite of the Landsat program. The observation bands are essentially the same seven bands as TM. The primary new features on Landsat 7 are a panchromatic band with 15 m spatial resolution, an on-board full aperture solar calibrator, 5% absolute radiometric calibration and a thermal IR channel with a four-fold improvement in spatial resolution over TM. An instrument malfunction occurred on May 31, 2003, with the result that all Landsat 7 scenes acquired since July 14, 2003 have been collected in "SLC-off" mode (https://landsat.usgs.gov/).

Landsat 8 carries two push-broom instruments: the Operational Land Imager (**OLI**), and the Thermal Infrared Sensor (TIRS). The spectral bands (Bands 2-8) of the **OLI** sensor, while similar to ETM+ sensor (Bands 1-5 and 7-8), provides enhancement from prior Landsat instruments, with the addition of two new spectral bands: a deep blue visible channel (Band 1 - Ultra Blue, 0.435 - 0.451 µm) specifically designed for water resources and coastal zone investigation, and a new infrared channel (Band 9 - Cirrus, 1.363 - 1.384 µm) for the detection of cirrus clouds. Thermal Band 10 (Thermal Infrared (TIRS 1, 10.60 - 11.19 µm)) and Band 10 (Thermal Infrared (TIRS 2, 11.50 - 12.51 µm)) are useful in providing more accurate surface temperatures and are collected at 100 meters (https://landsat.usgs.gov/).

The following figure shows the general view of detail of TM, ETM+ and OLI band designations.

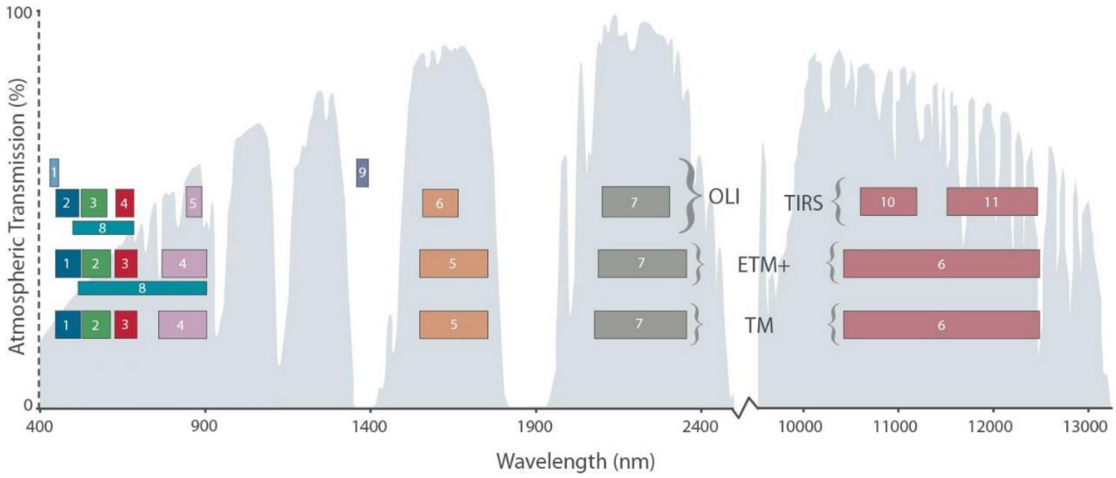

The band designations for all Landsat sensors (https://landsat.usgs.gov/).

The data quality (signal to noise ratio) and radiometric quantization (12-bits) of the OLI and TIRS is higher than previous Landsat instruments (8-bit for TM and ETM+), providing significant improvement in the ability to detect changes on the Earth’s surface. The principal functional differences between the ETM+ and the former TM series are the addition of a 15 m resolution panchromatic band and two 8-bit "gain" ranges. The goal of using two gain settings is to maximize the sensors' 8-bit radiometric resolution without saturating the detectors while the L4 & L5 TM radiometric calibration uncertainty of the at-sensor spectral radiances due to change of gains was around 5% and was somewhat worse (Chander et al., 2009).

The details and difference of Landsat TM, ETM+ and OLI were already analyzed in the manuscript (Page 7, lines 21-30; Page 8, lines 1-8; Page 15, lines 3-11; Page 30, Table 4).

References:

Chander, G., Markham, B. L., Helder, D. L.: Summary of current radiometric calibration coefficients for Landsat MSS, TM, ETM+, and EO-1 ALI sensors. Remote Sensing of Environment, 113, 893-903, doi:10.1016/j.rse.2009.01.007, 2009.

https://landsat.usgs.gov/what-are-band-designations-landsat-satellites

https://landsat.usgs.gov/how-does-landsat-8-differ-previous-landsat-satellites

https://earth.esa.int/web/sppa/mission-performance/esa-3rd-party-missions/landsat-1-7/tm-etm

Page 8 Section 2.3. It is not clear why atmospheric correction is needed, nor why the 6S method has been chosen above other methods.

Response:

For original remote sensing image, there are much signal at visible wavelengths from atmospheric path radiance, which prevents the proper interpretation of image (Chen et al., 2009), especially for water body of low reflectance. In order to derive the actual 'clear-sky' surface reflectance, the atmospheric correction is necessary before the application of remote sensing imageries (Gordon and Wang., 1994; Zhang et al., 2014). We have revised the statements to make it clearer (Page 9, lines 12-15).

As we all know, each of atmospheric correction methods has its advantages and disadvantages. Compared to the MODIS daily surface reflectance and Normalized Bidirectional Distribution Function-Adjusted Reflectance measurements, the global surface reflectance dataset from Landsat created by 6S-based atmospheric correction method has a high accuracy (Root-Mean-Squared Deviation: 1.3%-3.5%) (Feng et al., 2013; Maiersperger et al., 2013) (Page 9, lines 9, 12-15, 18-21). Thus, we chose the 6S method for atmospheric correction. We have revised the relevant statements in the manuscript (Page 9, lines 9, 12-15, 18-21).

References:
Chen, S., Huang, W., Wang, H., & Li, D.: Remote sensing assessment of sediment re-suspension during Hurricane Frances in Apalachicola Bay, USA. Remote Sensing of Environment, 113, 2670–2681, doi:10.1016/j.rse.2009.08.005, 2009.
Feng, M., Sexton, J.O., Huang, C., Masek, J.G., Vermote, E.F., Gao, F., Narasimhan, R., Channan, S., Wolfe, R.E., & Townshend, J.R.: Global surface reflectance products from Landsat: Assessment using coincident MODIS observations. Remote Sensing of Environment, 134, 276-293, 2013.
Gordon, H.R., & Wang, M.: Retrieval of water-leaving radiance and aerosol optical thickness over the oceans with SeaWiFS: a preliminary algorithm. Applied Optics, 33, 443-452, doi.org/10.1364/AO.33.000443, 1994.
Maiersperger, T.K., Scaramuzza, P.L., Leigh, L., Shrestha, S., Gallo, K.P., Jenkerson, C.B., & Dwyer, J.L.: Characterizing LEDAPS surface reflectance products by comparisons with AERONET, field spectrometer, and MODIS data. Remote Sensing of Environment, 136, 1-13, doi.org/10.1016/j.rse.2013.04.007, 2013.
Zhang, M., Dong, Q., Cui, T., Xue, C., & Zhang, S.: Suspended sediment monitoring and assessment for Yellow River estuary from Landsat TM and ETM+ imagery. Remote Sensing of Environment, 146, 136–147, doi.org/10.1016/j.rse.2013.09.033, 2014.

Page 9, Section 2.4. There is no justification for why all three assessment methods are needed or why they are chosen. Please clarify.

Response:

As the most frequently used methods (R^2, RMSE and MRE) for validation accuracy, we could found that the three assessment methods have been used to validate the accuracy of a model by many studies (Chen et al., 2009; Feng et al., 2014; Zhang et al., 2014). R-squared is conveniently scaled between 0 and 1, whereas RMSE is not scaled to any particular values. This can be good or bad; obviously R-squared can be more easily interpreted, but with RMSE we explicitly know how much our predictions deviate, on average, from the actual values in the dataset. So in a way, RMSE tells you more. Mean relative error (MRE) is one of the most common metrics used to measure accuracy for continuous variables. There used to be a time when there were a lot more published MRE results. It seems that publications I come across now mostly use either RMSE or some version of R-squared. In a word, the readers can conveniently compare the result with other studies when including all the three values. We have clarified the statements in the manuscript by adding the references (Page 10, lines 14-16).

References:
Chen, S., Huang, W., Wang, H., & Li, D.: Remote sensing assessment of sediment re-suspension during Hurricane Frances in Apalachicola Bay, USA. Remote Sensing of Environment, 113, 2670–2681, doi:10.1016/j.rse.2009.08.005, 2009.

Feng, L., Hu, C., Chen, X., & Song, Q.: Influence of the Three Gorges Dam on total suspended matters in the Yangtze Estuary and its adjacent coastal waters: Observations from MODIS. Remote Sensing of Environment, 140, 779–788, doi.org/10.1016/j.rse.2013.10.002, 2014.

Zhang, M., Dong, Q., Cui, T., Xue, C., & Zhang, S.: Suspended sediment monitoring and assessment for Yellow River estuary from Landsat TM and ETM+ imagery. Remote Sensing of Environment, 146, 136–147, doi.org/10.1016/j.rse.2013.09.033, 2014.

Page 9, section 3.1. It needs to be clearer why the reflectance in the red band and near infrared band is only used.

Page 9, Eqn3 – r is not defined in the numerator.

Response:

We are sorry that there are unclear statements about the Landsat sensors bands used. Actually, all bands (including red band and near infrared band) that the previous models used (Pages 28-29. Table 2) had been examined in the study. The relevant statements have been revised (Page 10, lines 10-11).

Page 9, equation (3) – r is the water surface reflectance measured in the field by ASD (350-2500 nm). We have revised the statements in manuscript (Page 10, line 10).

There is no discussion of the impact of sun glint and marine vessel contamination in the area (especially in the Pearl River estuary) – how is this dealt with?

Response:

The sun glint indeed has impact in estimating the concentration of water components. However, the influence of sun and sky glint, and vessel shadow on water surface reflectance could be avoided effectively based on above-water spectrum measurement method (Tang et al., 2004), which follows the community accepted standards and was applied widely (Feng et al., 2014; Zhang et al., 2014) (Page 7, lines 11-14).

Besides, the 6S atmospheric correction model used in this study has also corrected the skylight reflection (Sun and sky glint) following the Snell-Fresnel laws, environmental effects and directional target effects (Doxarana et al. 2002), and the Fresnel reflection is partially reduced by the presence of land in estuarial and coastal waters (Vidot and Santer 2005) (Page 9, lines 11-15).

There are about 7631×7801 pixels in one image and one pixel covers an area of about 900 m^2. We consider that the influence of the sampling platform (vessel) on the reflectance of remote sensing data was fairly small. The impact of sun glint and marine vessel contamination is really an interesting question and deserves the further study for accurate remote sensing reversion. We have made partial revision for the clarity (Page 7, lines 11-14; Page 9, lines 11-15). The following references have been added.

References:

Doxaran, D., Froidefond, J.M., Lavender, S., & Castaing, P.: Spectral signature of highly turbid waters Application with SPOT data to quantify suspended particulate matter concentrations. Remote Sensing of Environment, 81, 149-161, doi.org/10.1016/S0034-4257(01)00341-8, 2002.

Vidot, J., & Santer, R.: Atmospheric correction for inland waters-application to SeaWiFS. International Journal of Remote Sensing, 26, 3663-3682, DOI: 10.1080/01431160500034029, 2005.

The authors mention that they review and analyse 20 models (section 1) but only 5 models are discussed later (section 3.1), with little discussion about why only 5 were selected.

Response:

We do reviewed and analyzed 22 previous models (Pages 28-29. Table 2) mentioned in section 1 (Page 4, lines 25-26) based on the 119 in situ samples (Page 11, lines 4-5). We just selected the **five relatively better** models to show the results mainly based on the determination coefficient of calibration models (Page 11, lines 5-9; Page 32, figure 3) and the validation accuracy (Page 11, lines 11-18; Page 32, figure 3). In addition, the limitation of space in one page prevents us from showing more results (Page 11, lines 5-6; Page 32, figure 3).

Depth of samples and time of each sample should be mentioned.

Response:

We are sorry for that some information of samples had been summarized succinctly in **previous version**. The water samples and synchronous field spectral measurements were carried out from 10:00 to 15:00 (Page 7, lines 8-9). Water samples (about **1.5 L**) were collected within **1 m** water depth. Following your suggestions, we have revised the corresponding statements to make it clearer (Page 7, lines 1-19).

Some samples were taken from clear water (e.g. like the ones from Yangtze river estuary) which impacts reflectance due to higher amounts of water vapour and aerosols. This would need to be accounted for.

Some samples were taken from narrow canals with a width a bit bigger than TM spatial resolution. There would be an effect from the surrounding land on the reflectance of this water. This effect should be discussed.

Response:

The sampling method for the in-situ data in the study followed community accepted standards and was applied widely (Chen et al., 2015; Feng et al., 2014; Tang et al., 2004; Zhang et al., 2014), which could reduce the impact from water vapour and aerosols (Page 7, lines 11-14). The TSS concentrations of samples covered a large range of < 1 mg/L to >1000 mg/L in Yangtze River Estuary by the **same sampling method** (Feng et al., 2014). After all, TSS concentrations of offshore waters in Yangtze River Estuary were less than 20 mg/L usually (Feng et al., 2014). Following your suggestions, we have revised the statements to improve the manuscript.

There are some samples located in Zhongshan and Zhuhai (Page 29, figure 1d), which seems to be from narrow canals (Modaomen water way). However, Modaomen water way has the width of **500-1000 m** usually. The nearest distance from the samples to the surrounding land is more than **200 m**. We consider that there is a little of effect from the surrounding land on the reflectance of water body (Page 7, lines 14-16).

References:

Chen, J., Quan, W., Cui, T., & Song, Q.: Estimation of total suspended matter concentration from MODIS data using a neural network model in the China eastern coastal zone. Estuarine, Coastal and Shelf Science, 155, 104-113, doi.org/10.1016/j.ecss.2015.01.018, 2015.

Feng, L., Hu, C., Chen, X., & Song, Q.: Influence of the Three Gorges Dam on total suspended matters in the Yangtze Estuary and its adjacent coastal waters: Observations from MODIS. Remote Sensing of Environment, 140, 779–788, doi.org/10.1016/j.rse.2013.10.002, 2014.

Tang, J., Tian, G., Wang, X., Wang, X., & Song, Q.: The Methods of Water Spectra Measurement and Analysis: Above-Water Method. Journal of Remote Sensing, 8, 37-44, 2004.

Zhang, M., Dong, Q., Cui, T., Xue, C., & Zhang, S.: Suspended sediment monitoring and assessment for Yellow River estuary from Landsat TM and ETM+ imagery. Remote Sensing of Environment, 146, 136–147, doi.org/10.1016/j.rse.2013.09.033, 2014.

There was minimal variability in sampling locations in each estuary/coastal area. Samples were taken either in areas which were turbid or clear, despite there being wider ranging turbidity in the area.

The selection of sampling locations should be discussed, with comment on why the sampling locations tended to be clustered in this way.

Response:

Sampling locations covering wide ranging of turbidity, are important to the study of variation of TSS concentrations in estuaries and coasts. Thus, samples of the study were taken from the river downstream towards the sea (including shoals, channels, maximum turbidity zones) mainly based on the wide TSS changes of each estuary/coastal area.

In our study areas, Xuwen coast is **a less turbid region** due to less water discharge, sediment load and protection of coral reef (Page 5, lines 7-10). The mean distance of two samples is more than 0.8 km and the farthest distance is about 23.98 km (Page 31, figure 1b), which covers a large area of Xuwen coast (10.77%), including two core areas and a buffer area in Xuwen Coral Reef Reserve. TSS concentrations of the 32 samples ranges from **4.3 mg/L** to **37.8 mg/L** with a mean value of **11.2 mg/L** in Xuwen coast. These samples represent the variability of TSS concentrations in the region well.

TSS concentrations in Moyangjiang River Estuary, Pearl River Estuary and Hanjiang River Estuary of Guangdong Province (Page 31, figure 1c, d, e) were mainly affected by the interaction of runoff and tide. So, the samples in the three estuaries (Page 31, figure 1c, d, e) with the **almost same representativeness** were carried out from the **lower river reaches** to the **outer shelf area (**including shoals, channels, maximum turbidity zones). TSS concentrations of the total of 62 simples (Page 31, figure 1c, d, e) in the three estuaries ranging from **5.2 mg/L** to **220.7 mg/L**. Among them, TSS concentrations of 15 simples ranges from 106 mg/L to 220.7 mg/L with a mean value of **150.9 mg/L**. In addition, the mean distance of two samples and the farthest distance from lower river reaches in the three estuaries are more than 0.7 km and about **15.3 km** in Moyangjiang River Estuary (Page 31, figure 1c), 1.3 km and **27.4 km** in Pearl River Estuary (Page 31, figure 1d) and 0.7 km and **8.7 km** in Hanjiang River Estuary (Page 31, figure 1e), respectively. We believe that the samples can reflect the characteristic of turbidity of estuaries of Guangdong Province well.

Besides, TSS concentrations of the 34 samples in Yangtze Estuary (Page 31, figure 1f) ranges from **38.4 mg/L** to **577.2 mg/L** with a mean value of 178.2 mg/L. The mean distance of two samples is more than **2.6 km** and the farthest distance from lower river reaches is about **73.32 km** (Page 31, figure 1f). These samples reflect the large variation of TSS concentrations of Yangtze River well.

Following your suggestions, we have added the statements to discuss and illustrate the representativeness of the location or concentrations of the samples (Page 7, lines 1-4).

It is better to mention that root mean square of Trimble global positioning system is related to real time or post processed accuracy (page 6 line 21)

Response:

The root mean square error of Trimble global positioning system is related to real time. We have revised the statement to make it clearer. (Page 7, line 1).

The process of matching image and sample points should be discussed.

Response:

Similar to previous studies (Bailey and Werdell. 2006; Chen et al., 2015; Zhang et al., 2014), the process of producing the satellite data for comparison with the in situ measurements was based on the positions of the samples recorded by Trimble global positioning system and considered the **two-hour** time window around the satellite overpass (Page 8, line 26; Page 8, lines 10-12, 21-22; Page 15, lines 15-18).

References:

Bailey, S.W., & Werdell, P.J.: A multi-sensor approach for the on-orbit validation of ocean color satellite data products. Remote Sensing of Environment, 102, 12-23, doi.org/10.1016/j.rse.2006.01.015, 2006.

Chen, J., Quan, W., Cui, T., & Song, Q.: Estimation of total suspended matter concentration from MODIS data using a neural network model in the China eastern coastal zone. Estuarine, Coastal and Shelf Science, 155, 104-113, doi.org/10.1016/j.ecss.2015.01.018, 2015.

Zhang, M., Dong, Q., Cui, T., Xue, C., & Zhang, S.: Suspended sediment monitoring and assessment for Yellow River estuary from Landsat TM and ETM+ imagery. Remote Sensing of Environment, 146, 136–147, doi.org/10.1016/j.rse.2013.09.033, 2014.

Section 3.2, page 12 line 12. I am not clear how the vertex values have been calculated. This should be clarified.

Response:

We are sorry for the omission of the calculation of the vertex values. We have added the following contents and revised the statements to make the calculation of the vertex values clearly. (Page 13, lines 16-21).

Firstly, we can get the derivative (equation (2)) from equation (1) by calculus. Then, we can obtain the vertex point through solving the roots of the derivative (equation (2)). Finally, the vertex values can be calculated by the parameters. Parameters a, b and c corresponding to OLI, ETM+ and TM sensors are -0.3575, 1.1135, 0.7162, -0.2844, 0.8578, 0.8278 and -0.2821, 0.8506, 0.8295, respectively (Page 34, figure 4). The unit of TSS concentration is in mg/L. So, the vertex values are 36.08633 mg/L (~36.1 mg/L) for OLI, 32.21716 mg/L (~32.2 mg/L) for ETM+ and 32.18162 mg/L (~32.2 mg/L) for TM (Page 13, lines 19-20).

$$\frac{Log(R_1)}{Log(R_2)} = a*(\mathrm{Log}(TSS))^2 + b*\mathrm{Log}(TSS) + c \quad (1)$$

$$\left(\frac{Log(R_1)}{Log(R_2)}\right)' = 2a*(Log(TSS))+b$$

$$\Rightarrow \text{Log}(TSS) = -\frac{b}{2a} \qquad (2)$$

$$\Rightarrow TSS = 10^{-\frac{b}{2a}}$$

Page 18, line 1. New results have been introduced in the summary and conclusions. These should be in the body of the text or in figures first.

Response:

Now we have revised some statements on the validation of QRLTSS model from Landsat imageries to illustrate these results (Section 3.4. Page 17, lines 17-20). In fact, the results are not new findings. These results had already been shown in figure 7d (Page 37).

Technical corrections

There are numerous grammatical and structural issues that should be addressed. This manuscript would benefit from editing and review from a native English speaker to improve structure, flow and readability.

Response:

Thanks a lot for the valuable comments about the grammatical and structural issues. Following your suggestions, we have asked for **two native speakers** (associated professors of USA) helping us to pick up grammatical errors and revise the manuscript very carefully. **In addition**, reviewer #1 had also helped to point out main writing errors and structural issues and revised our manuscript carefully. In the revision process, the linkages had been polished and added in the manuscript for the improvement of the flow between sentences, and paragraphs, improving the understanding of the general modelling strategy (Page 3, line 19; Page 15, line 14; Page 6, lines 21-25; Page 9, lines 2-4; Section 2.1; Section 2.4; Section 2.5; Section 3.4). The contents of "extraction of water bodies" in Section 3.4 is removed to Section 2.1 (Page 6). The contents of the "Band response function application of Landsat sensors for field spectra" in Section 3.1 have been moved to Section 2.4 (Page 10). All the revising have been marked in red in the marked-up mode (Page 1, lines 1-2, 14-15, 17-23, 25-28; Page 2, lines 1-2, 5-6, 10; Page 3, lines 1-4, 15-16, 18-19, 26; Page 4, lines 20-22, 24-27; Page 5, lines 9-10, 17-18, 22-23; Page 6, lines 5-6, 13-14, 21-25; Page 7; Page 8, lines 1-6, 10-15, 17, 22, 26-27; Page 9, lines 1-3, 7-9, 12-15, 18-21; Page 10, lines

10-11, 14-16; Page 11, lines 6-7; Page 12, lines 2-4; Page 13, lines 14-21, 24; Page 14, lines 18-19; Page 15, lines 6-9, 19-22; Page 16, lines 4-9, 16, 26-27; Page 17, lines 6-7, 17-20, 23-24; Page 18, lines 4-5, 14, 19-23, 27; Page 19, lines 1-4, 6, 9-10, 17, 21-23).

Section 2.2, I would recommend the dates being in day month year order to make them easier to read/follow.

Response:

We have revised the statements of the dates in section 2.2 to make them easier to read and checked the manuscript following your suggestions. (Page 7, lines 4-8, 10, ; Page 8, lines 13-15, 17, 22; Page 15, lines 18-21; Page 16, line 4).

Sentences should not start with the word 'And'

The writing is sometimes too conversational. For example, page 4 line 20 "What's more" could be replaced with "furthermore".

Response:

Thanks for the comments. We have checked the manuscript carefully and revised the sentences that start with the word "And" (Page 4, lines 20-22, 26-27; Page 13, line 24; Page 15, lines 6-7; Page 16, lines 7-9).

Following your suggestions, we have revised the statements (Page 4, lines 20-22) that you pointed out and modified relevant writing of the whole manuscript carefully from native speakers.

Tables 1-3 could be easier to read if each section was more clearly separated. For example, table 1, it is not clear what dates and samples are specific to Region c. Table 2, it is difficult to tell which turbidity models are used for TM 1,3, 4 as opposed to TM, 1,2,3,4. Table 3, I suggest adding a line between the previous models and the ones used in this study: : :etc

Figure 1 should go from a to e rather than e,a,b,c,d, as is currently the case. Need to make it clearer in the caption that the black dots are the sampling locations. Please explain the difference between circles and triangle in figure 1c (page 21).

Response:

Following your suggestions, we added horizontal lines to the tables 1-3 for separating each section more clearly. Indeed, they are easier to read after the improvement.

We have revised the figure 1 (goes from a to e) and make it clearer that the **black dots and triangles** are all the sampling locations in the caption (Page 31). There are **40 samples** (dots and triangles) in figure 1c. Among them, the field **spectral measurements** and synchronous water samples (TSS concentrations) of **30 samples (dots)** were collected (Page 7, lines 8-9). Another **ten**

samples (triangles) in figure 1c have the **TSS concentrations collected only** (Page 7, lines 9-11). With or without synchronous spectral measurements is the difference between circles and triangles in figure 1c (Page 31).

The revised tables 1-3 and figure 1 has also been shown as follows.

Once again, thank you very much for your valuable comments and suggestions for the improvement of the manuscript!

The revised Table 1. Information about the study areas and in-situ data

Location	Hydrologic features (length, drainage area, mean surface runoff and sediment discharge)	Date	Samples	Measurements	Number of synchronous samples with satellite
Region I	—, — $8.6 \cdot 10^8 m^3$/year, $3 \cdot 10^4$ ton/year	Dec 3, 2010	10	Reflectance, TSS	No
		Jan 13~14, 2013	22	Reflectance, TSS	No
Region II	199 km, $6 \cdot 10^3$ km^2, $8.21 \cdot 10^9$ m^3/year, $3.27 \cdot 10^5$ ton/year	Dec 6, 2013	11	Reflectance, TSS	7, OLI
Region III	2320 km, $4.53 \cdot 10^5$ km^2, $3.26 \cdot 10^{11}$ m^3/year, $7.53 \cdot 10^7$ ton/year	Dec 19, 2006	5	Reflectance, TSS	No
		Dec 21, 2006	18	8 samples with Reflectance and TSS; 10 samples with TSS only	13, Hyperion
		Dec 27, 2007	8	Reflectance, TSS	No
		Nov 2, 2012	9	Reflectance, TSS	6, ETM+
Region IV	470 km, $3.01 \cdot 10^4$ km^2, $2.45 \cdot 10^{10}$ m^3/year, $6.93 \cdot 10^6$ ton/year	Dec 1, 2013	12	Reflectance, TSS	9, OLI
Region V	6280 km, $1.8 \cdot 10^6$ km^2, $9.2 \cdot 10^{11}$ m^3/year, $4.8 \cdot 10^8$ ton/year	Oct 14~15, 2009	34	Reflectance, TSS	No

The revised Table 2. Review of previous TSS or Turbidity retrieval models using Landsat imagery.

Data	Model	Study area	Reference
TM Bands 2, 4	TSS=29.022•exp(0.0335•(B4/B2))	Gironde and Loire Estuaries	Doxaran et al. (2003)
MSS Bands 5, 6	$\mathrm{Ln(TSS)}= 1.4\cdot(B5/B6)^{2}-6.2\cdot(B5/B6)+10.8$	the Bay of Fundy and the Beaufort Sea	Topliss et al. (1990)
TM Bands 1, 3, 4	Turbidity=11.31•(B4/B1)-2.03•B3-16.42	Chagan Lake	Song et al. (2011)
TM Band 4	Turbidity=16.1•B4-12.7	Nebraska Sand Hills Lakes	Fraser. (1998)
TM Band 3	Turbidity=10•B3-24.8		
TM Band 1	Turbidity=19•B1-97.9		
TM Band 2	Turbidity=6.4•B2-28		
TM Band 3	TSS=69.39•B3-201	Ganges and Brahmaputra Rivers	Islam et al. (2001)
MSS Bands 1, 2	$\mathrm{Ln(TSS)}= 2.71\cdot(B1/B2)^{2}-9.21\cdot(B1/B2)+8.45$	Enid Reservoir in North Central Mississippi	Ritchie and Cooper. (1991)
TM Band 3	Log(TSS)= 0.098•B3+0.334	Delaware Bay	Keiner and Yan. (1998)
TM Bands 2, 3	TSS=0.7581•exp(61.683•(B2+B3)/2)	southern Frisian lakes	Dekkera et al. (2001)
TM Bands 1, 3	TSS=0.0167•exp(12.3•B3/B1)	an embayment of Lake Michigan	Lathrop et al. (1991)
TM/ETM+ Band 3	Log(TSS)= 44.072•B3 +0.1591	Yellow River estuary	Zhang et al. (2014)
TM Band 3	TSS=2.19•exp(21.965•B3)	Poyang Lake	Wu et al. (2013)
	$\mathrm{TSS}=-9275.78\cdot(B3)^{3}+8623.19\cdot(B3)^{2}-810.04\cdot B3+23.44$		
TM Bands 3, 4	$\mathrm{TSS}=5829.8\cdot(B3-B4)^{3}+4165.09\cdot(B3-B4)^{2}-189.88\cdot(B3-B4)+5.43$		
	TSS=3.411•exp(21.998•(B3-B4))		
OLI Bands 2, 3, 8	TSS=-191.02•B2+36.8•B3+172.66•B8+4.57	Xin'anjiang Reservoir	Zhang et al. (2015)
TM	B2=0.0044•TSS+2.5226	Bhopal	Rao et al. (2009)

Band 2		Upper Lake	
TM Band 2, 3	Log(TSS)= 6.2244•(B2+B3)/B2•B3+0.892	Yangtze estuary	Li et al. (2010)
TM Band 3	TSS=0.543•B3-7.102	Beysehir Lake	Nas et al. (2010)
TM Band 4	$TSS=229457.695•(B4)^2+146.462•B4+5.701$	Bohai gulf	Chen et al. (2014)

The revised Table 3. The comparison of calibration and validation accuracy of several best TSS retrieval models

Model form		Calibration (R^2)	Validation (RMSE(mg/L), MRE)		
			Whole	Low range	High range
Chen et al. (2014)		0.7842	35.7, 144.2%	18.35, 215.58%	53.56, 23.5%
Li et al. (2010)		0.6167	69.3, 45%	5.66, 52.6%	113.48, 32.1%
Zhang et al. (2014)		0.5804	82.8, 48%	6.56, 53.9%	135.54,38.15%
Lathrop et al. (1991)		0.6661	50.3 39.4%	6.12, 44.6%	82.09, 30.57%
Ritchie and Cooper. (1991)		0.6983	68.7, 41.3%	7.24, 44%	112.32, 36.6%
This study	OLI	0.7181	21.5, 27.2%	3.5, 31.1%	35.1, 20.7%
	ETM+	0.708	25, 32.5%	4.6, 38.3%	40.7, 20.3%
	TM	0.7079	24.9, 31.5%	4, 35.3%	40.6, 25.1%

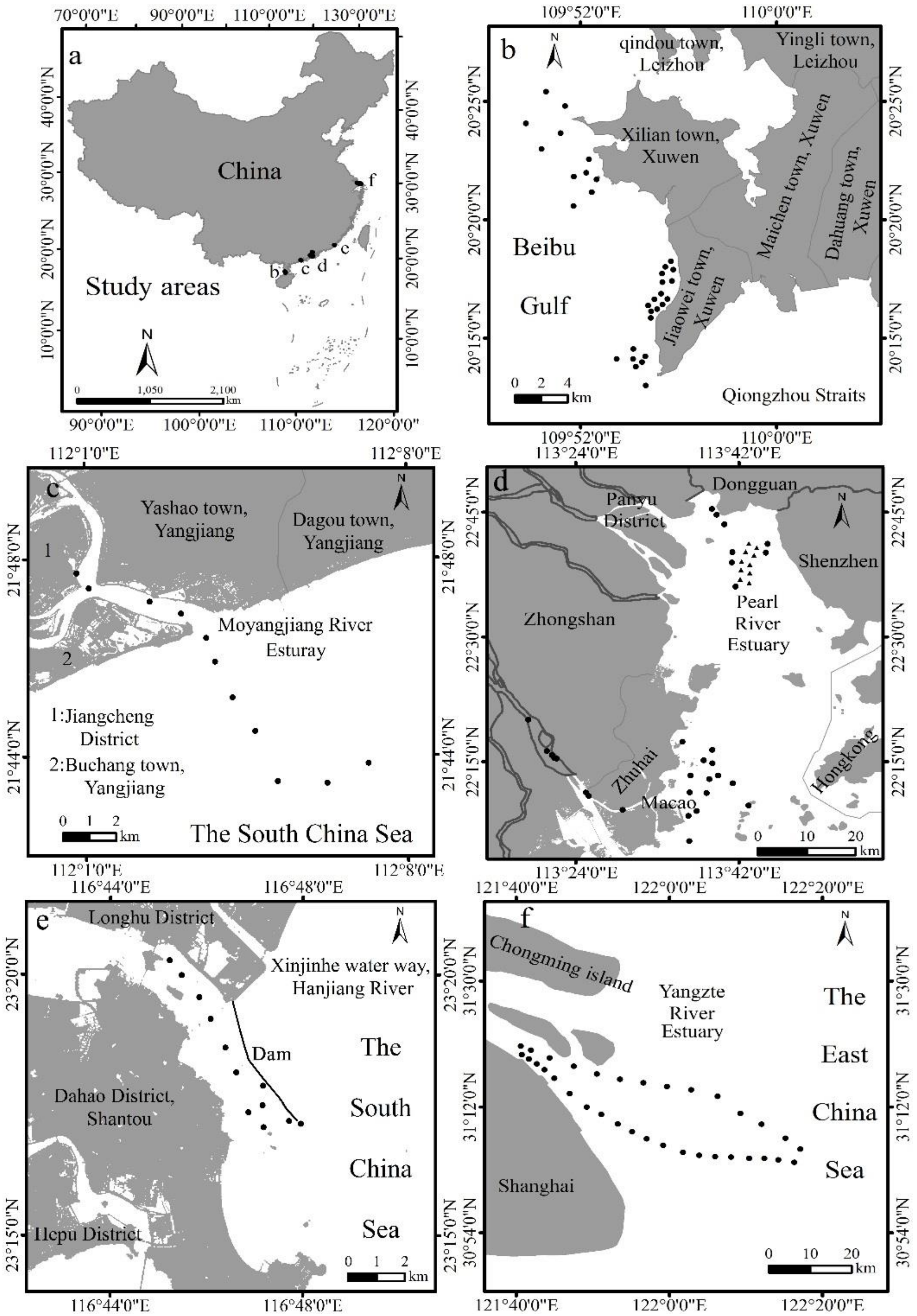

The revised Figure 1. Study areas and locations of in situ data (black dots and triangles). b: Xuwen coast; c: Moyangjiang River Estuary; d: Pearl River Estuary; e: Hanjiang River Estuary; f: Yangtze River Estuary.

A Landsat-based model for retrieving total suspended solids concentration of estuaries and coasts in China

Chongyang Wang[1,2,3], Shuisen Chen[2], Dan Li[2], Wei Liu[1,2,3], Ji Yang[1,2,3], Danni Wang[4]

[1] Guangzhou Institute of Geochemistry, Chinese Academy of Sciences, Guangzhou 510640, China

[2] Guangzhou Institute of Geography, Guangzhou 510070, China

[3] University of Chinese Academy of Sciences, Beijing 100049, China

[4] Department of Resources and the Urban Planning, Xin Hua College of Sun Yat-Sen University, Guangzhou 510520, China

Correspondence to: Shuisen Chen (css@gdas.ac.cn)

Abstract. Retrieving total suspended solids (TSS) concentration accurately is essential for sustainable management of estuaries and coasts, which plays a key role in the interaction of hydrosphere, pedosphere and atmosphere. Although many TSS retrieval models have been published, the general inversion method that is applicable to different field conditions is still under research. In order to obtain a TSS remote sensing model that is suitable for estimating TSS concentrations with wide range in estuaries and coasts by Landsat imageries, after reviewing a number of Landsat-based TSS retrieval models and improving a relatively better one among them, this study developed a Quadratic model using the Ratio of Logarithmic transformation of red band and near infrared band and logarithmic transformation of TSS concentration (QRLTSS) based on 119 in-situ samples collected in 2006-2013 from five regions of China. It was found that the QRLTSS model works well and shows a satisfactory performance. The QRLTSS model based on Landsat TM, ETM+ and OLI sensors explained about 72% of the TSS concentration variation (TSS: 4.3-577.2 mg/L, N=84, P-value < 0.001) and had an acceptable validation accuracy (TSS: 4.5-474 mg/L, RMSE ≤ 25mg/L, N=35). In addition, a threshold method of red band reflectance (OLI: 0.032, ETM+ and TM: 0.031) was proposed to solve the two-valued issue of the QRLTSS model and to retrieve TSS concentration from Landsat imageries. After 6S model-based atmospheric correction of Landsat OLI and ETM+ imageries, the TSS concentrations of three regions (Moyangjiang River Estuary, Pearl River Estuary and Hanjiang River Estuary) in Guangdong Province of China were mapped by the QRLTSS model. The results indicated that TSS concentrations in the three estuaries showed large variation ranging from 0.295 mg/L to 370.4 mg/L. Meanwhile we found that the Landsat imageries inversed TSS concentrations showed good validation accuracies with synchronous water samples (TSS: 7-160 mg/L, RMSE: 11.06 mg/L, N=22). The further validation from EO-1 Hyperion imagery also showed good performance

(in-situ synchronous measurement of TSS: 106-220.7 mg/L, RMSE: 26.66 mg/L, N=13) of the QRLTSS model for the area of high TSS concentrations in Lingding Bay of Pearl River Estuary. Evidently, the QRLTSS model is potentially applied to simulate high-dynamic TSS concentrations of other estuaries and coasts by Landsat imageries, improving the understanding of the spatial and temporal variation of TSS concentrations on regional and global scales. Furthermore, the QRLTSS model can be optimized to establish a regional or unified TSS retrieval model of estuaries and coasts in the world for different satellite sensors with medium- and high- resolution similar to Landsat TM/ETM+/OLI sensors or with similar red band and near infrared band, such as ALI, HJ-1 A/B, LISS, CBERS, ASTER, ALOS, RapidEye, Kanopus-V, GF.

Keywords: total suspended solids, estuaries and coasts, QRLTSS model, Landsat, remote sensing

1 Introduction

Total suspended solids (TSS) is a critical factor of the ecological environment of water bodies, which directly and deeply affects their optical properties through absorbing and scattering of the sunlight (Chen et al., 2015b; Pozdnyakov et al., 2005; Wang et al., 2016; Wu et al., 2013), leading to impacts on the primary production of the water areas (May et al., 2003). Estuaries and coasts are the most important intermediate zones that connect hydrosphere, pedosphere and atmosphere, which then pass on a deep and wide impact on many aspects of our societal and natural environment (Nechad et al., 2010; Pozdnyakov et al., 2005). The topic of TSS concentration monitoring and spatial and temporal variation assessment has been paid great attention, and the associated research work has been conducted frequently by a variety of scholars, government branches and society communities (Caballero et al., 2014; Giardino et al., 2015; Liu et al., 2003; Lu et al., 2012; Montanher et al., 2014; Nechad et al., 2010; Olmanson et al., 2013; Pozdnyakov et al., 2005; Rao et al., 2009; Shen et al., 2008; Tang et al., 2004b; Zhang et al., 2007). Many methods can be used to estimate TSS concentrations of water bodies, including hydrological sites monitoring, in-situ investigation, physical models, numerical simulation, remote sensing and so on (Chen et al., 2015a). Retrieving TSS concentrations from remote sensing data has unique advantages due to the wide spatial coverage and periodic revisit, such as Land Observation Satellite (Landsat), the first Earth Observing (EO-1), the Moderate Resolution Imaging Spectroradiometer (MODIS), the Medium Resolution Imaging Spectrometer (MERIS), the Geostationary Ocean Color Imager (GOCI), the Sea Viewing Wide Field of View Sensor (SeaWiFS), Systeme Probatoire d'Observation dela Tarre (SPOT) and the

Environment and Disaster Monitoring and Forecasting Small Satellite Constellation (HJ). Compared to other remote sensing data, Landsat series of imageries have advantage on spatiotemporal dynamics analysis of TSS concentrations (Wu et al., 2013) due to the additional good quality, high spatial resolution and inheritance, especially long-term historical data since 1972.

Many Landsat-based models have estimated the TSS concentration with empirical, semi-empirical, semi-analytical or analytical algorithms (Chen et al., 2014; Doxaran et al., 2003; Fraser., 1998; Islam et al., 2001; Li et al., 2010; Montanher et al., 2014; Nas et al., 2010; Oyama et al., 2009; Raharimahefa and Kusky., 2010; Rao et al., 2009; Ritchie and Cooper., 1991; Topliss et al., 1990; Volpe et al., 2011; Wang et al., 2016; Wu et al., 2013; Zhang et al., 2014). Based on the rigorous theoretical derivation, the semi-analytical and analytical models are likely more applicable to different water bodies than the empirical or semi-empirical methods (Binding et al., 2012; Binding et al., 2010; Chen et al., 2015b; Giardino et al., 2007; Ma et al., 2010; Sipelgas et al., 2009). However, there are still limitations of the application due to the difficulties of retrieval or inaccuracies on initialization parameters (Binding et al., 2012; Chen et al., 2015b; Ma et al., 2010; Wu et al., 2013). Therefore, the empirical, especially semi-empirical methods are still used to estimate TSS concentration, and will continue to be used for a long time due to their simplicity and sufficient accuracies. It should be noted that the applications of empirical or semi-empirical TSS models need to be revalidated in different regions and periods because they are largely region-, time- or environment dependent (Wu et al., 2013). We found that previous empirical or semi-empirical Landsat-based TSS retrieval models vary greatly in their main forms of single band or multiple bands for different estuaries and coasts (Ma et al., 2010; Wu et al., 2013).

The TSS models of single band include linear function (Fraser., 1998; Islam et al., 2001; Nas et al., 2010; Rao et al., 2009), exponential or logarithmic function (Keiner and Yan., 1998; Wu et al., 2013; Zhang et al., 2014) and quadratic function (Chen et al., 2014). Those models have been applied to many regions easily because they not only have the simple forms but also more choice of remote sensing data. We know that the sensitivity of satellite sensor bands is different for different TSS concentrations. Many studies have proven that reflectance in the red band increases with the increasing of TSS concentrations, but tends to convergence or keeps stable due to saturation effect under high TSS concentrations (Ritchie and Zimba., 2005; Feng et al., 2014), while the reflectance in the near infrared band is more sensitive to high TSS concentrations compared to low TSS concentrations (Chen et al., 2015b; Feng et al., 2014; Hu et al., 2004; Wang et al., 2010). Thus, those models of single band have limited applications in regions with wide dynamic range of TSS concentration.

Models of multiple bands combination worked better than a single band in avoiding the effect of saturation for water bodies of high TSS concentrations, and have been applied widely (Dekkera et al., 2001; Doxaran et al., 2003; Feng et al., 2014; Montanher et al., 2014; Oyama et al., 2009; Wang et al., 2016). Although the bands combination includes band ratio (Doxaran et al., 2003; Lathrop et al., 1991; Ritchie and Cooper., 1991; Topliss et al., 1990; Wang et al., 2016) and other complex forms (Dekkera et al., 2001; Li et al., 2010; Oyama et al., 2009; Song et al., 2011; Zhang et al., 2015), these models of multiple bands combination can be also classified into linear, exponential, logarithmic or quadratic function. Besides quadratic forms of models (Chen et al., 2014; Ritchie and Cooper., 1991; Topliss et al., 1990), most of those empirical or semi-empirical TSS retrieval models are simple monotonic functions. Monotonic function has some potential issues. One is that the change of band reflectance corresponds to the fixed change of TSS concentrations, which may be unrealistic, such as linear function. Another is that a little change of band reflectance can cause exaggerated estimation of TSS concentrations, such as exponential and logarithmic function. Although some non-monotonic functions could avoid the potential issues, it is widely believed that there does not exist a regional or universal empirical or semi- empirical TSS retrieval model for all water bodies (Ma et al., 2009; Tang et al., 2005; Wu et al., 2013).

Recently, we published a short conference paper (Wang et al., 2016), which stated that the quadratic TSS model could be a new method for estimating the wide-range TSS concentrations of multiple estuaries and coasts. However, the model lacks necessary analysis and discussion of results due to limitation of space. Besides, our previous model (Wang et al., 2016) could not be applied to remote sensing data for the reason that each value of reflectance does not correspond to a unique TSS concentration.

Based on the above analysis, this study intends to develop a Landsat-based model with better adaptability and robustness for retrieving TSS concentrations in estuaries and coasts. To achieve this goal, the applicability of more than 20 previous Landsat-based models was reviewed and further analyzed. We focus on the models of multiple bands combination, and the form of models belongs to non-monotonic function. This paper was organized as follows. In-situ data, pre-processing and Landsat imageries were described along with the atmospheric correction method and assessment method of simulation model accuracy in Section 2. The TSS retrieval model, validation and the spatial analysis of TSS concentration mapped from Landsat imageries and EO-1 Hyperion imagery were presented in Section 3. Finally, the summary and conclusions were given in Section 4.

2 Materials and methods

2.1 Study areas

The study areas including five regions of China are listed as follows.

Region I, Xuwen coast (Fig.1b), located between longitudes 109.8°~110.1°E and latitudes 20.1°~20.5°N, is the important Coral Reefs National Nature Reserve with the most plentiful coral species because of its less turbid waters. The good water quality is due to less water discharge ($8.6 \bullet 10^8 m^3$/year on average) and sediment load ($3 \bullet 10^4$ ton/year on average) and protection of coral reef (Wang et al., 2002). It was reported that the coral reefs does not grow as well as before (Zhao et al., 2011). Researchers believe that this is mainly caused by the increasing TSS concentration, declination of water transparency, and decreasing water temperature due to excessive fish farming, overfishing and industrial pollution (Chen et al., 2015b). The coastal land development is also an important reason.

Region II, Moyangjiang River Estuary (Fig.1c), is located between longitudes 112°~112.2°E and latitudes 21.65°~21.9°N, southwest of Guangdong Province. The source of Moyangjiang River is in Yangchun County, and it has a length of 199 km and a drainage area of more than $6 \bullet 10^3$ km^2. The annual mean surface runoff of Moyangjiang River is $8.21 \bullet 10^9 m^3$ and sediment load is $3.27 \bullet 10^5$ ton/year on average. Moyangjiang River crosses Yangchun, Yangdong and Jiangcheng Counties (Districts) and flows into the South China Sea.

Region III, Pearl River Estuary (Fig.1d), is located between longitudes 113.15°~114.1°E and latitudes 21.9°~23°N. Pearl River is the fourth longest (2320 km) in China with a drainage area of $4.53 \bullet 10^5$ km^2, and its annual runoff ($3.26 \bullet 10^{11} m^3$) is only smaller than Yangtze River. The sediment load of Pearl River is $7.53 \bullet 10^7$ ton/year on average. Pearl River crosses eight water ways, (Humen, Jiaomen, Hongqimen, Hengmen, Modaomen, Jitimen, Hutiaomen and Yamen) located at six cities of Guangdong Province and pours into South China Sea. As we all know estuary and coast of Pearl River suffers severely from combined pollution (Ma and Wang 2003) which mainly comes from industrial production, residential life and seawater intrusion (Chen et al., 2009a).

Region IV, Hanjiang River Estuary (Fig.1e), is located between longitudes 116.6 °~117 °E and latitudes 23.2 °~23.6 °N, east of Guangdong Province and southwest of Fujian Province. Hanjiang River has a length of 470 km and has the second largest drainage area ($3.01 \cdot 10^4$ km^2) in Guangdong Province. The annual mean surface runoff of Hanjiang River is $2.45 \cdot 10^{10}$m^3 with sediment load is $6.93 \cdot 10^6$ ton/year on average. The lower reaches of Hanjiang River include Beixi water way located in northeast, Dongxi water way located in the middle and Xixi water way located in the west. Xixi water way also crosses with the three water ways of Waishahe, Xinjinhe and Meixi, and flows into the South China Sea. Waishahe, Xinjinhe and Meixi water ways are located in east, middle and west of Longhu District, Shantou of Gungdong Province, respectively.

Region V, Yangtze River Estuary (Fig.1f), is located between longitudes 121.55 °~122.4 °E and latitudes 30.8 °~31.8 °N. Yangtze River is the largest river in China, and has a length of 6280 km and a drainage area of $1.8 \cdot 10^6$ km^2. The annual mean surface runoff of Yangtze River is $9.2 \cdot 10^{11}$m^3 with sediment load is $4.8 \cdot 10^8$ ton/year on average (Feng et al., 2014). Such huge terrestrial input not only loads to its extremely turbid waters but also impacts on the optical properties of this region. It is reported that the environment of Yangtze River estuary is getting worse due to the rapid developments and urbanization in the surrounding industrial areas (Chen et al., 2015a; Hsu and Lin., 2010). As a result, there are more and more studies focusing on this region due to its important ecological and economic role (Chen et al., 2015a; Feng et al., 2014; Shen et al., 2010).

Water bodies of the study areas were extracted based on method developed by Jiang et al (2014). The difference of spectral profile across water and cloud were used to mask clouds (Chen et al., 2009; Chen et al., 2011a). We find that the reflectance of water is usually less than 0.05 in near infrared band while the reflectance of cloud is usually more than 0.1 in near infrared band in the study areas. Thus, the clouds were masked based on reflectance that is more than 0.05 in near infrared band.

2.2 In-situ and satellite data

The 129 in-situ samples were collected from the above-mentioned five regions of China, and their positions were recorded by Trimble global positioning system (real time) with root mean square errors of 1~4 m (shown in Fig.1). Samples of the study were taken from a river downstream towards the sea (including shoals, channels, maximum turbidity zones) mainly based on the wide TSS changes of each estuary/coastal area for representing the wide variability of TSS concentrations (Fig.1b, c, d, e, f, dots and triangles). Among the 129 samples, 32 samples were collected from Xuwen coast on 3rd December 2010 and 13th to 14th February 2013; 11 samples were collected from Moyangjiang River Estuary on 6th December 2013; 40 samples were collected from Pearl River Estuary on 19th, 21st December 2006, 27th December 2007 and 2nd November 2012; 12 samples were collected from Hanjiang River Estuary on 1st December 2013; 34 samples were collected from Yangtze River Estuary on 14th to 15th October 2009. The field spectral measurements and synchronous water samples of the above-mentioned 119 samples were carried out from 10:00 to 15:00 (Fig.1b, c, d, e, f, dots. Table 1). Besides, another ten samples with TSS concentrations from Pearl River Estuary on 21st December 2006 were collected synchronously with Earth-observing (EO-1) Hyperion imagery only (Fig.1d, triangles. Table 1). The spectrum were measured based on above-water spectrum measurement method that could avoid the influence of sun and sky glint, water vapour, aerosols, and vessel shadow effectively (Tang et al., 2004a), which was applied to the water bodies like estuaries and coasts of China widely (Chen et al., 2015a; Feng et al., 2014; Zhang et al., 2014). It should be noted that the distance from some samples (located in Zhongshan and Zhuhai. Fig.1d) taken from Modaomen water way to the surrounding land is more than 200 m usually. Thus, there is a little of effect from the surrounding land on the reflectance of water body. Finally, the reflectance of water surface (Fig.2) was calculated in the same way as Zhang et al. (2014) and Chen et al. (2015b) did. Water samples (about 1.5 L) were collected within the water depth of 1m, and TSS concentrations were measured by a weighed method (Binding et al., 2012; Caballero et al., 2014).

TM, ETM+ and OLI sensors onboard the Landsat 5, 7 and 8 satellites, respectively, have a spatial resolution of about 30m, with more than seven band spanning from visible to infrared wavelength. The spectral bands of the OLI sensor, while similar to TM and ETM+ sensor, provides enhancement from prior Landsat instruments, with the addition of two new spectral bands: a deep blue visible channel (band 1) specifically designed for water resources and coastal zone investigation, and a new infrared channel (band 9) for the detection of cirrus clouds. A new Quality Assurance band is also included with each data product. This provides information on the presence of features such as clouds, water, and snow (https://landsat.usgs.gov/). The data quality (signal to noise ratio) and radiometric quantization (12-bits) of the OLI and TIRS is higher than previous Landsat instruments (8-bit for TM and ETM+), providing significant improvement in the ability to detect changes on the Earth's surface. The principal functional differences between the ETM+ and the former TM series are the addition of a 15 m resolution panchromatic band and two 8-bit "gain" ranges. The ETM+ images are acquired in either a low-or high-gain state. The goal of using two gain settings is to maximize the sensors' 8-bit radiometric resolution without saturating the detectors while the L4 & L5 TM radiometric calibration uncertainty of the at-sensor spectral radiances due to change of gains was around 5% and was somewhat worse (Chander et al. 2009). However, after the revision of gains, Landsat imageries can basically be fit for quantifying the optical properties in oceans, lakes, estuaries and coasts which have been explored in many studies although they were originally designed for observation of land targets (Montanher et al., 2014; Nas et al., 2010; Volpe et al., 2011; Wu et al., 2013; Zhang et al., 2014).

Due to frequent cloud coverage in estuaries and coasts, as well as the low temporal resolution (16d) of Landsat satellite (Bailey and Werdell., 2006), this study obtained three Landsat imageries with good quality only that can be matched with synchronous in-situ measurements of three study regions (Table 1). The first scene of image from ETM+ (path/row = 122/45) was captured on 2nd November 2012, covering part of Pearl River Estuary (Fig.1d). The second scene of image (path/row = 120/44) from OLI was captured on 1st December 2013, covering Hanjiang River Estuary (Fig.1e). The third scene of image (path/row = 123/45) from OLI was captured on 6th December 2013, covering Moyangjiang River Estuary (Fig.1c). It should be noted that the scan line corrector (SLC) of Landsat 7 ETM+ has failed since 31st May 2003. However, there are still many research works using the SLC-off data that is repaired using local self-adaptive regression analysis (Zhang et al., 2014). The repaired data in our study is provided by the International Scientific Data service Platform, Computer Network Information Center, Chinese Academy of Sciences (http://datamirror.csdb.cn).

In addition, a scene of EO-1 Hyperion image (path/row=122/44) was captured on 21st December 2006, covering part of Pearl River Estuary (Fig.1d). With spectral coverage ranging from 400 to 2500 nm and 10 nm (sampling interval) of contiguous bands of the solar reflected spectrum, Hyperion's spatial resolution is 30 m with a 7.7 km imagery swath and 185 km length (http://eo1.usgs.gov). Hyperion is also well suited for retrieving spatial distributions of water-color constituents in Pearl River Estuary (Chen et al., 2009a). The Hyperion data was used for further validation of TSS retrieval model here.

2.3 Atmospheric correction method

There are much signal at visible wavelengths from atmospheric path radiance, which prevents the proper interpretation of original image (Chen et al., 2009), especially for water body of low reflectance. Thus, the atmospheric correction is a necessary step before the remote sensing inversion (Gordon and Wang., 1994; Zhang et al., 2014). The commonly used methods of atmospheric correction include the simple Dark Object Subtraction (DOS), Fast Line-of-sight Atmospheric Analysis of Spectral Hypercubes (FLAASH), and Second Simulation of Satellite Signal in the Solar Spectrum (6S) models. In addition, the regression analysis of spectral bands is also a common method used for atmospheric correction (Chen et al., 2011a; HEDLEY et al., 2003; Hochberg et al., 2003; Mei et al., 2001; Montanher et al., 2014). All in all, each of atmospheric correction methods has its advantages and disadvantages.

The 6S code the study used is the improved version of Simulation the Satellite Signal in the Solar Spectrum (5S), developed by the Laboratoire d'Optique Atmospherique (Vermote et al., 1997). The 6S atmospheric correction model can also correct the skylight reflection (Sun and sky glint) following the Snell-Fresnel laws, environmental effects and directional target effects (Doxarana et al. 2002), and the Fresnel reflection is partially reduced by the presence of land in estuarial and coastal waters (Vidot and Santer 2005). The 6S code is frequently used for atmospheric correction of Landsat imageries based on the Landsat Ecosystem Disturbance Adaptive Processing System (LEDAPS, a Landsat atmospheric correction codebase funded by NASA's Terrestrial Ecology Program) (Feng et al., 2013; Ju et al., 2012; Maiersperger et al., 2013; Masek et al., 2006). Compared to the MODIS daily surface reflectance and Normalized Bidirectional Distribution Function-Adjusted Reflectance measurements, the global surface reflectance dataset from Landsat created by LEDAPS has a high accuracy (Root-Mean-Squared Deviation: 1.3%-3.5%) (Feng et al., 2013; Maiersperger et al., 2013). Thus, the LEDAPS software was chosen for atmospheric correction in this study. We assumed the continental aerosol type because the northeast monsoon was blowing from the land in the study. The aerosol optical thickness was derived independently from each Landsat acquisition using the dark dense vegetation (DDV) approach (Kaufman and Tanré, 1996). Critical atmospheric parameters of 6S model, including water vapor at a resolution of 2.5 by 2.5 degrees (http://dss.ucar.edu/datasets/ds090.0/) and ozone concentrations at a resolution of 1.25 longitude and 1 latitude, were collected from National Centers for Environmental Prediction (NCEP) and Total Ozone Mapping Spectrometer (TOMS) or NOAA's Television Infrared Observation Satellite Program (TIROS) Operational Vertical Sounder (TOVS), respectively (Feng et al., 2013; Ju et al., 2012; Masek et al., 2006). Rayleigh scattering was adjusted to local conditions by a static 0.05 degree digital topography dataset (derived from the 1 km GTopo30) and NCEP surface pressure data (Feng et al., 2013; Masek et al., 2006). All the parameters are automatically called corresponding to each Landsat image when LEDAPS runs.

2.4 Band response function application of Landsat for field spectra

Before establishing TSS retrieval model, the water surface reflectance measured in the field was convoluted with the Landsat band response functions to derive the band-weighted reflectance data using equation (1). It is also a critical step for the application of TSS retrieval model from ground spectral data to remote sensing imageries.

$$R(\text{band}) = \frac{\sum_{band_{\min}}^{band_{\max}} f(\lambda_{band}) r(\lambda_{band})}{\sum_{band_{\min}}^{band_{\max}} f(\lambda_{band})} \qquad (1)$$

Where, $band_{min}$ and $band_{max}$ are the lower and upper limits of Landsat band in red and near infrared bands, respectively. $r(\lambda)$ is the water surface reflectance; $f(\lambda)$ is the spectral response function of Landsat sensors (http://Landsat.usgs.gov). The simulated "R(band)", corresponding to all bands of Landsat OLI, ETM+/TM, was calculated for each spectrum.

2.5 Accuracy assessment method of models

In order to validate the accuracy of the TSS spectral models, atmospheric correction and mapping of TSS concentrations, the most frequently used methods (Chen et al., 2009; Feng et al., 2014; Zhang et al., 2014), including the determination coefficient (R^2), the root mean square error (RMSE) and mean relative error (MRE), were also used in the study for convenience of comparison by different readers.

$$RMSE = \sqrt{\frac{\sum_{i=1}^{i=n} \left(x_i - x_i^{'}\right)^2}{n}} \qquad (2)$$

$$MRE = \frac{\sum_{i=1}^{i=n} \left| \frac{x_i - x_i^{'}}{x_i} \right|}{n} \times 100\% \qquad (3)$$

Where x_i is the observed value, x_i' is the modeled value, i is the i th element, and n is the number of elements.

3 Results and discussions

3.1 Evaluation of previous Landsat-based TSS models

The previous Landsat-based TSS retrieval models (Table 2) were calibrated and validated again with the optimization of parameters based on the 119 in-situ samples (84 in-situ samples for calibration, the other 35 for validation). There were five relatively better results of simulation presented in Fig.3 only due to the limitation of page space. The results indicated that the previous Landsat-based TSS models did not explain the TSS variation so well. The determination coefficient of calibration models in the five better TSS models (Fig.3) was between 0.58 and 0.784, corresponding to linear (Fig.3c1) and quadratic (Fig.3a1) model of single band, respectively.

The five TSS retrieval models were further validated based on another 35 in-situ samples with range of 4.5-474 mg/L. The results showed that minimum MRE was 39.4% from exponential model of single band (Fig.3d2), but its RMSE was 50.26 mg/L. The quadratic model of single band (Fig.3a2) got minimum RMSE (35.73 mg/L) but with high MRE value of 144.2%. Obviously, the quadratic model of single band is hard to be adopted for this study. However, for the exponential model of single band, the high RMSE prevented this form of model from applying as well, especially when we took the TSS concentration of 22 validation data (lower than 36 mg/L, Fig.3 in triangles) into account. The RMSEs and MREs of the other three forms of models were 69.3 mg/L and 45%, 82.7 mg/L and 48% for linear model (Fig.3b2 and c2), 68.7 mg/L and 41.3% for quadratic model (Fig.3e2), respectively. In contrast, the non-monotonic function, quadratic model of ratio of bands (Fig.3e) had a better performance among the five examined TSS models. But, we still expect that there would be a TSS model with high calibration and validation accuracy simultaneously for estuaries and coasts of China by Landsat imageries.

3.2 Development of QRLTSS model

In order to develop a Landsat-based model with higher calibration and validation accuracy, some MODIS-based TSS retrieval models (Chen et al., 2009b; Chen et al., 2011ab; Chen et al., 2015b; Wang et al., 2010) were referred. These models made full use of the relationship between the ratio of logarithmic transformation of red band and near infrared band and logarithmic transformation of TSS concentration. Thus, following the feature of these MODIS based models, we improved the model (Fig.3e1) that developed by Ritchie and Cooper. (1991), under MATLAB environment, shown in Fig.4.

From Fig.3 and Fig.4 (a1, b1 and c1), we found that the quadratic model of the ratio of logarithmic transformation of red band and near infrared band and logarithmic transformation of TSS concentration (QRLTSS, equation (4)) has a higher calibration accuracy than most of the previous TSS models, no matter whether it is Landsat OLI, ETM+ or TM sensor.

$$\frac{Log(R_1)}{Log(R_2)} = a*(\mathrm{Log}(TSS))^2 + b*Log(TSS) + c \qquad (4)$$

Where R_1 and R_2 represent near infrared band and red band of OLI, ETM+ and TM sensors. Parameters a, b and c refer to Fig.4, respectively. The unit of TSS concentration is in mg/L.

Compared to the previous model developed by Ritchie and Cooper. (1991), we improved the input with logarithmic transformation of bands and made full use of the different sensitivity of red and near infrared bands to TSS concentrations that have been proved by many studies (Chen et al., 2015b; Feng et al., 2014; Wang et al., 2010; Hu et al., 2004). Compared to the MODIS-based models developed by Chen et al. (2011b) and Wang et al. (2010), the QRLTSS model established in this paper seems more complicated. The models (Chen et al., 2011b; Wang et al., 2010) are in linear or exponential form, belonging to simple monotonic function that can cause unreliable estimation in some spectral range. Although the QRLTSS model developed in our study is similar to previous studies (Chen et al., 2009b; Chen et al., 2011a; Chen et al., 2015b), there are some differences among them. They are indeed all quadratic models, but the models developed by Chen et al. (2009b) and Chen et al. (2011a) are part of the curve. It is different from the form developed by Chen et al. (2015b) and this study, which are all complete quadratic curve. It should be noted that the part of quadratic model has limitation in estimating TSS concentration with the wide range. Some regions with lower or higher TSS concentration could not be retrieved accurately. In fact, TSS concentrations in the study area (Apalachicola Bay, USA) of Chen et al. (2009b) and Chen et al. (2011a) are not as high as TSS concentrations in study areas of this paper and Chen et al. (2015b). The maximum TSS concentration in the previous studies was about 200 mg/L (Chen et al., 2009b; Chen et al., 2011a), but the maximum TSS concentration was more than 500 mg/L (Yangtze

River Estuary) for previous study (Chen et al., 2015b) and this study. In addition, the study areas of Chen et al. (2015b) only include Xuwen Coral Reef National Nature Reserve, a less turbid region, and Yangtze River Estuary, an extremely turbid region, which might make the model developed by Chen et al. (2015b) perform worse in the middle of the quadratic curve than both ends of the quadratic curve. The QRLTSS model in this study is better in the continuity of calibration and validation data than Chen et al. (2015b). The reason is that the study areas of this paper include not only their regions (Chen et al., 2015b) but also other three main estuarine regions, Guangdong province (Moyangjiang River Estuary, Pearl River Estuary and Hanjiang River Estuary). In general, the TSS concentrations in the three additional regions are higher than Xuwen coast, but lower than Yangtze River Estuary. These data are good supplement for the robustness of an accurate model on the previous study.

It should be noted that a band value corresponds to two TSS concentrations values based on the QRLTSS model (equation (4)). We should make the unique choice when validating or retrieving TSS concentration by the model. Unfortunately, we had not been aware of this problem and did not solve it in our previous work (Wang et al., 2016). It meant that our previous results (Wang et al., 2016) were not complete. In this study, the TSS concentrations of vertex corresponding to the three quadratic models based on Landsat OLI, ETM+ and TM sensors have been obtained through solving the equation (4) as follows. Firstly, the derivative were calculated from equation (4) by calculus. Then, we can obtained the vertex point through solving the root of the derivative by the parameters (Fig.4. a, b, c for OLI: -0.3575, 1.1135, 0.7162; ETM+: -0.2844, 0.8578, 0.8278; TM: -0.2821, 0.8506, 0.8295). Finally, the vertex values were calculated out. The vertex value for OLI is about 36.1 mg/L. The vertex values for ETM+ and TM are about 32.2mg/L, which attribute to their almost same spectral band features (Table 4).

$$\left(\frac{Log(R_1)}{Log(R_2)}\right)' = 2a*(\mathrm{Log}(TSS)) + b$$
$$\Rightarrow \mathrm{Log}(TSS) = -\frac{b}{2a}$$
$$\Rightarrow TSS = 10^{-\frac{b}{2a}}$$

For QRLTSS model based on OLI sensor, we found that the values of OLI red band weighted reflectance of all validation data are lower than 0.032 when TSS concentrations are less than 36.1 mg/L (Fig.5a, blue dots) except for one exceptional data (Fig.5a, black dot). The reflectance is higher than 0.032 when TSS concentrations are more than

36.1 mg/L (Fig.5a, red dots). The QRLTSS models based on ETM+ and TM sensor have similar situations. But the values of TSS concentration and reflectance at vertex are 32.2 mg/L and 0.031, shown in Fig.5b (dots for ETM+ and triangles for TM). The findings are different from the result found in MODIS-based model by Chen et al. (2015b). In previous study (Chen et al., 2015b), the values of TSS concentration and reflectance of MODIS red band at vertex are 31 mg/L and 0.025, respectively. We believe that the difference was caused by different spectral characteristics of satellite sensors (Table 4). This is also why multi-source satellite remote sensing becomes more and more important in recent years. Monitoring TSS concentrations from multiple data sources could make full use of the advantages of all kinds of satellite sensors. According to the above analysis, TSS concentration can be retrieved by using equation (5) in the form of positive squared root if the reflectance of red band is lower than 0.032 (OLI sensor) or 0.031 (ETM+ and TM sensors), and using equation (5) in the form of negative squared root if the reflectance of red band is greater than 0.032 (OLI sensor) or 0.031 (ETM+ and TM sensors), respectively.

$$Log(TSS)=\frac{-b\pm\sqrt{b^2-4a\left(c-\frac{Log(R_1)}{Log(R_2)}\right)}}{2a},\left(b^2-4a\left(c-\frac{Log(R_1)}{Log(R_2)}\right)\geq 0\right) \quad (5)$$

We validated the QRLTSS model based on the 35 in-situ samples and the selection criteria (equation (5)). The results indicated that the QRLTSS model has a better performance than the previous five TSS models although QRLTSS model explained about 72% of the TSS concentration variation only. The RMSEs and MREs of all validation data for QRLTSS model are 21.5 mg/L and 27.2% for OLI (Fig.4a2), 25 mg/L and 32.5% for ETM+ (Fig.4b2), and 24.9 mg/L and 31.5% for TM (Fig.4c2), respectively. All of the simulated results from QRLTSS model have higher validation accuracies than the best of the five previous TSS models (RMSE: 35.7 mg/L, MRE: 39.4%). According to the vertex location of the quadratic model, the wide range of validation data (TSS: 4.5-474 mg/L) was divided into two parts of low (4.5-32.2 mg/L, triangles in Fig.3 and Fig.4) and high (36.2-474 mg/L, squares in Fig.3 and Fig.4) TSS concentration for further validation. For the data of low TSS concentrations, the RMSEs and MREs of validation are 3.5 mg/L and 31.1% for OLI, 4.6 mg/L and 38.3% for ETM+, and 4 mg/L and 35.3% for TM. For the data of high TSS concentrations, the RMSEs and MREs of validation are 35.1 mg/L and 20.7% for OLI, 40.7 mg/L and 20.3% for ETM+, and 40.6 mg/L and 25.1% for TM. The validation accuracies of the two parts are still better than the best of the previous five TSS models (RMSEs & MREs: 5.6 mg/L & 39.4% for low concentration part, and 53.5 mg/L & 23.5% for high concentration part). The detailed information of calibration and validation in Fig.3 and Fig.4 were shown in Table 3.

From Table 3 we could also find that the calibration and validation accuracy of OLI-based QRLTSS model is a little higher than ETM+ and TM (R^2: 0.7181 vs 0.708 and 0.7079, RMSE: 21.5 mg/L vs 25 mg/L and 24.9 mg/L, MRE: 27.2% vs 32.5% and 31.5%). We attribute this mainly to the improvement of Landsat OLI sensor's design. Especially for OLI band_5, the band of water vapor absorption at 825 nm was removed from the near infrared band range, whose wavelength is 845-885 nm now (http://Landsat.usgs.gov/Landsat8.php). However, the near infrared band wavelength of ETM+ and TM are 775-900 nm and 760-900 nm, respectively. In addition, the red band wavelength of OLI is 630-680 nm, and the correspondence of ETM+ and TM is 630-690 nm. The little difference between ETM+ and TM sensors determines a little difference in QRLTSS model based on ETM+ and TM. The performance (red band and near infrared band) of different sensors and the vertexes of the QRLTSS model based on these sensors were shown in Table 4.

3.3 Comparison of Landsat measured reflectance with in-situ reflectance

In order to analyze the spatial and temporal variation of TSS concentrations in our study areas and further verify accuracy of QRLTSS model, the acquired Landsat imageries were used to calculate the TSS concentrations by the QRLTSS model described in Section 3.2 (Equation (5)). Atmospheric correction is critical for working with multi-scene imageries and empirical/semi-empirical methods. Thus, the atmospheric correction accuracy of 6S was calculated firstly based on the reflectance of synchronous in-situ measurements, a total of 22 samples from three regions within two-hour time window of satellite overpass (Bailey and Werdell. 2006; Chen et al., 2015; Zhang et al., 2014). Among them, six of the total 22 samples were collected from Pearl River Estuary on 2nd November 2012, nine samples were collected from Hanjiang River Estuary on 1st December 2013 and the other seven samples were collected from Moyangjiang River Estuary on 6th December 2013. In deriving the reflectance comparison, the water-leaving radiances from Landsat imageries were averaged by window of 3×3 pixels of the location of the sample of the image. We then calculated RMSE and MRE of the reflectance result after atmospheric correction with in-situ reflectance. RMSEs and MREs of red and near infrared bands are 0.0033, 9.58% and 0.00092, 21.5%, respectively, which showed an acceptable accuracy. The results in Fig.6 shows that the 6S model was sufficiently stable and accurate for deriving the reflectance at visible and near infrared band from Landsat satellite data for the purpose of remote sensing applications in estuarine and coastal waters.

3.4 Validation of QRLTSS model from Landsat imageries

After atmospheric correction of 6S, the TSS concentrations of Moyangjiang River Estuary, part of Pearl River Estuary, Hanjiang River Estuary were estimated from ETM+ or OLI imageries (Fig.7). Fig.7a showed the TSS concentrations in Moyangjiang River Estuary (Beijing time at 11:00) on 6th December 2013 with a large variation ranging from 0.557 mg/L to 203.9 mg/L. It is clear that the TSS concentrations are higher inside and outside of Moyangjiang River Estuary than outer shelf area, especially in the downstream estuary, with a mean value of 154.2 mg/L (Fig.7a). The region of high TSS concentrations in Moyangjiang River Estuary looks lung-shaped. The outer shelf area has low TSS concentrations, where the TSS concentrations less than 35 mg/L were frequently found and the maximum is not more than 60 mg/L. So, there are sharp fronts that could be seen clearly between coastal area and outer shelf area. The TSS distribution in Moyangjiang River Estuary mainly attribute to interaction of tide and runoff. In this study, the remote sensing imagery covering Moyangjiang River Estuary was obtained at 11:00 in the morning when the tide had begun to ebb and runoff with large amounts of sediment flowed into the South China Sea.

Different from TSS concentrations in Moyangjiang River Estuary, the TSS concentrations in eastern Zhuhai & Macao and Hongkong coastal water bodies are with much lower TSS at a mean value of ~12 mg/L (Fig.7b. Blank areas without synchronous image). There was a significant decreasing trend of TSS concentration from the northwest to southeast of Pearl River Estuary. It was mainly due to the interaction between runoff (flowing towards southwest) and tide (flowing towards northwest). The maximum TSS concentration was about 29 mg/L. The reason why the water bodies in outer Lingding Bay of Pearl River Estuary had a low level TSS concentration was probably because of strong management protection and less human activity. Most part of eastern Zhuhai water bodies belong to Pearl River Estuary Chinese White Dolphin National Nature Reserve (NNR) since 2003 (http://www.gdofa.gov.cn/). The NNR has an area of about 460 km^2 located between longitudes 113.66°~113.87°E and latitudes 21.18°~22.4°N, shown in Fig.7b (region with black dotted line). The low TSS concentrations in this region confirms the protection effect of Chinese White Dolphin.

Compared to Moyangjiang River Estuary and eastern Zhuhai and Macao coastal water bodies, the TSS concentrations in Hanjiang River Estuary had wider variables, ranging from 0.295 to 370.4 mg/L. The water bodies with high TSS concentrations in this region were mainly in two zones where the sharp fronts of TSS were clearly visible (Fig.7c, zones 1 and 2). The TSS concentrations in zone 1 were almost more than 100 mg/L with maximum value of 370.4 mg/L and a mean value of 167.91 mg/L. For zone 2, the TSS concentrations mostly ranged from 20 mg/L to 110 mg/L, and the maximum and mean value were 127.14 mg/L and 61.57 mg/L. The results also showed that the turbid river runoff flows into South China Sea along east coast of Dahao District, Shantou City. The high TSS concentrations in this region were caused by different factors. In zone 1 at opposite bank of Dahao District, Shantou, it was mainly caused by the runoff of Xixi waterway, Hanjiang River and the flow guiding line (Dam, solid black line in Fig.1e and Fig.7c) connected to Longhu District, Shantou City. While in zone 2, the high TSS concentrations were resulted from the interaction of tide current and runoff, which is the potential location of estuarine barrier bar. The TSS concentrations in estuary of Xinjinhe waterway, Hanjiang River were less than 50 mg/L. The results are similar to the results of Ding and Xu (2007), which showed TSS concentrations ranged from 0.1 mg/L to 300 mg/L in Hanjiang River Estuary.

The accuracy of TSS concentration estimated from Landsat imageries of two OLIs and one ETM+ was further validated with 22 quasi synchronous in-situ samples that were collected from Pearl River Estuary, Hanjiang River Estuary and Moyangjiang River Estuary. The validation accuracy was shown in Fig.7d. The RMSE and MRE of comparison between 22 field TSS concentrations (7-160 mg/L) and Landsat satellite inversion are 11.06 mg/L and 24.1%, respectively. In addition, the RMSEs and MREs of validation for the low range (7-28.2 mg/L, N=18) and the high range (37-160 mg/L, N=4) of TSS concentrations in the three estuaries are 3.75 mg/L and 22%, 24.69 mg/L and 33.2%, respectively. These results indicated that the QRLTSS model is applicable to the mapping of TSS in all of three estuaries from Landsat imageries.

3.5 Further validation of QRLTSS model from EO-1 Hyperion imagery

We were fortunate to acquire a scene of EO-1 Hyperion imagery at 10:33 (Beijing time) with synchronous 13 samples (Fig.1d. ten sites with symbol of triangles and three sites with symbol of dots. Table 1. TSS: 106-220.7 mg/L) on 21st December 2006 covering part of Pearl River Estuary from northeast to southwest of the Lingding Bay. The data set gives us an opportunity to further validate the accuracy of the QRLTSS model. After similar pre-processing steps with Landsat imageries, the EO-1 Hyperion imagery was also used to retrieve TSS concentrations using the QRLTSS model. The results of TSS concentration mapping and validation accuracy were shown in Fig.8.

The TSS concentration mapping from Hyperion image on December 21, 2006 ranged from 1.79 mg/L to 361.6 mg/L, with a mean value of 124.4 mg/L (Fig.8a). The mapping results of TSS showed large variation from northeast to southwest in Pearl River Estuary. The areas of low TSS concentration were detected near the southwest of Lingding Bay (mostly in NNR, Fig.7b) and in deep channels (east channel and west channel, Fig.8a) of Lingding Bay. The areas of high TSS concentration were in accordance with the outlets of different waterways (Humen, Jiaomen, Hongqimen and Hengmen) of Pearl River Estuary frequently or the foreshores, which indicate that it is the maximum turbidity zones of the estuary. The 13 synchronous samples (TSS: 106-220.7 mg/L) were mostly collected from the northern zone of high TSS concentrations (Fig.1d). Comparisons of accuracy validation between in-situ and Hyperion imagery inversed TSS concentrations were produced in Fig.8b. The RMSE and MRE of comparison are 26.66 mg/L and 12.6%, respectively. It showed that the QRLTSS model also worked well in area of high TSS concentrations from Hyperion mapping result of Pearl River Estuary.

Based on the evaluation and analysis of all the above results (Fig. 3, 4, 7 and 8. Table 3 and 4), we conclude that the QRLTSS model has the advantage for quantitative inversion of TSS concentrations with a high dynamic range in estuaries and coasts. These results explained the usability of QRLTSS model by the validation of multi-spectral Landsat OLI/ETM+ and hyperspectral EO-1 Hyperion imageries compared to our previous work (Wang et al., 2016).

4 Summary and conclusions

This study developed a QRLTSS model with high adaptability and robustness for estimating wide TSS concentration variables of estuaries and coasts from Landsat imageries (TSS: 4.3-577.2 mg/L, R^2: ~0.72, N=84, P-value < 0.001). The QRLTSS model got a reasonable validation accuracy by the independent in-situ samples (TSS: 4.5-474 mg/L, RMSE $\leq$ 25 mg/L, N=35). Compared to the 22 previous Landsat-based models (Table 2), the QRLTSS model has better performance (Table 3). In addition, we found that the QRLTSS model based on the bands of OLI showed a higher accuracy than bands of ETM+ and TM (Table 3 and Fig.4), which can be explained by the adjusted band design of OLI sensor in reducing the effect of water vapor absorption compared to ETM+ and TM sensors (Table 4).

The QRLTSS model showed good performance when applied to estimate TSS concentrations from Landsat OLI/ETM+

imageries (Fig.7). The RMSEs and MREs of validation from Landsat imageries (Moyangjiang River Estuary, December 6, 2013; part of Pearl River Estuary, November 2, 2012 and Hanjiang River Estuary, December 1, 2013) are 11.06 mg/L and 24.1% for the whole range (7-160 mg/L), 3.75 mg/L and 22% for the low range (7-28.2 mg/L), and 24.69 mg/L and 33.2% for the high range (37-160 mg/L) of TSS concentrations, respectively. Besides, the high validation accuracy of TSS mapping from Hyperion imagery of Pearl River estuary (December 21, 2006) with in-situ data (106-220.7 mg/L) using the QRLTSS model had also been obtained (Fig.8, RMSE: 26.66 mg/L, MRE: 12.6%).

Landsat imageries could be one of the best choices in terms of the availability of data source for remote sensing of TSS in estuaries and coasts, considering the spatial resolution and acquirement of long time series (30m TM/ETM+/OLI beginning in 1982, 80m MSS since 1972). The research shows that the QRLTSS model can quantify the TSS concentration variation of estuaries and coasts by Landsat series of imageries with applicable accuracies (R^2: 0.71-0.72, 30m), which can be compared to the accuracies of previous OLI/ETM+/TM based studies (R^2: 0.67-0.92, 30m (Chen et al., 2014; Nas et al., 2010)) and MODIS-based studies (R^2: 0.61-0.86, 250m (Chen et al., 2011a; Wang et al.,2010)). The TSS concentrations at vertex of QRLTSS model based on Landsat sensors are different from MODIS (Table 4). Based on the vertex of QRLTSS model, we proposed a threshold (corresponding to the vertex of quadratic function) of red band reflectance (Fig.5, OLI: 0.032, ETM+ and TM: 0.031) which can be used to divide the quadratic function for solving the QRLTSS model under two kinds of squared roots (Table 4).

For a lot of medium- and high- resolution remote sensing sensors similar to Landsat series satellites, such as HJ-1 A/B, LISS, CBERS, ASTER, ALOS, RapidEye, Kanopus-V, GF, we deduce that there is potential to optimize the QRLTSS model for mapping the wide range TSS concentrations of estuaries and coasts from multi-source satellite remote sensing. It will be beneficial to the understanding of the spatial and temporal variation of TSS concentrations on regional and global scales, and providing great help in establishing regional or unified TSS remote sensing model of estuaries and coasts in the world.

Code and data availability

The LEDAPS code used for atmospheric correction and all the remote sensing imageries are fully available in the supplement to the article.

Acknowledgments

This research was supported by Science & Technology Plan Project of Guangdong Province (2014A020216027, 2016A020223011), Technology transformation project of Zhongshan City-Guangdong Academy of Sciences (2016G1FC0017) and the Water Conservancy Science & Technology Innovation Project (2011-20). The authors would like to thank USGS for providing the Landsat imagery. Thanks are also given to the International Scientific Data Service Platform, Computer Network Information Center, Chinese Academy of Sciences for providing gap filled ETM+ SLC-off data (http://datamirror.csdb.cn).

References

Bailey, S.W., & Werdell, P.J.: A multi-sensor approach for the on-orbit validation of ocean color satellite data products. Remote Sensing of Environment, 102, 12-23, doi.org/10.1016/j.rse.2006.01.015, 2006.

Binding, C.E., Greenberg, T.A., & Bukata, R.P.: An Analysis of MODIS-Derived Algal and Mineral Turbidity in Lake Erie. Journal of Great Lakes Research, 38, 107-116, doi.org/10.1016/j.jglr.2011.12.003, 2012.

Binding, C.E., Jerome, J.H., Bukata, R.P., & Booty, W.G.: Suspended particulate matter in Lake Erie derived from MODIS aquatic colour imagery. International Journal of Remote Sensing, 31, 5239-5255, DOI: 10.1080/01431160903302973, 2010.

Caballero, I., Morris, E.P., Ruiz, J., & Navarro, G.: Assessment of suspended solids in the Guadalquivir estuary using new DEIMOS-1 medium spatial resolution imagery. Remote Sensing of Environment, 146, 148–158, doi.org/10.1016/j.rse.2013.08.047, 2014.

Chander, G., Markham, B. L., Helder, D. L.: Summary of current radiometric calibration coefficients for Landsat MSS, TM, ETM+, and EO-1 ALI sensors. Remote Sensing of Environment, 113, 893-903, doi:10.1016/j.rse.2009.01.007, 2009.

Chen, J., Quan, W., Cui, T., & Song, Q.: Estimation of total suspended matter concentration from MODIS data using a neural network model in the China eastern coastal zone. Estuarine, Coastal and Shelf Science, 155, 104-113, doi.org/10.1016/j.ecss.2015.01.018, 2015a.

Chen, S., Fang, L., Zhang, L., & Li, D.: Remote sensing of turbidity in seawater intrusion reaches of Pearl River estuary: A case study in Modaomen waterway of Pearl River estuary，China. Estuarine，Coastal and Shelf Science, 82, 119-127, doi:10.1016/j.ecss.2009.01.003, 2009a.

Chen, S., Han, L., Chen, X., Li, D., Sun, L., & Li, Y.: Estimating wide range Total Suspended Solids concentrations from MODIS 250-m imageries: An improved method. ISPRS Journal of Photogrammetry and Remote Sensing, 99, 58–69, doi.org/10.1016/j.isprsjprs.2014.10.006, 2015b.

Chen, S., Huang, W., Wang, H., & Li, D.: Remote sensing assessment of sediment re-suspension during Hurricane Frances in Apalachicola Bay, USA. Remote Sensing of Environment, 113, 2670–2681, doi:10.1016/j.rse.2009.08.005, 2009b.

Chen, S., Huang, W.R., Chen, W.Q., & Chen, X.Z.: An enhanced MODIS remote sensing model for detecting rainfall effects on sediment plume in the coastal waters of Apalachicola Bay. Marine Environmental Research, 72, 265–272, doi:10.1016/j.marenvres.2011.09.014, 2011a.

Chen, S., Huang, W.R., Chen, W.Q., & Wang, H.Q.: Remote sensing analysis of rainstorm effects on sediment concentrations in Apalachicola Bay, USA. Ecological Informatics, 6, 147–155, doi:10.1016/j.ecoinf.2010.12.001, 2011b.

Chen, Y., Kong, J., Sun, X., Du, D., & Cheng, P.: Retrieval of sea surface suspended sediment concentration in Bohai Gulf Offshore area based on semi-analysis model. Geography and Geo-Information Science, 30, 33-36,55, doi:10.3969/j.issn.1672-0504.2014.03.008, 2014.

Dekkera, A.G., Vosb, R.J., & Petersb, S.W.M.: Comparison of remote sensing data, model results and in-situ data for total suspended matter žTSM/ in the southern Frisian lakes. The Science of the Total Environment, 268, 197-214, DOI: 10.1016/S0048-9697(00)00679-3, 2001.

Ding, X., & Xu, X.: A remote sensing analysis of characteristics of Suspended sediments movement in Hanjiang estuary. REMOTE SENSING FOR LAND & RESOURCES, 3, 71-74, doi:10.3969/j.issn.1001-070X.2007.03.016, 2007.

Doxaran, D., Froidefond, J.M., & Castaing, P.: Remote-sensing reflectance of turbid sediment-dominated waters. Reduction of sediment type variations and changing illumination conditions effects by use of reflectance ratios. Applied Optics, 42, 2623-2634, DOI: 10.1364/AO.42.002623, 2003.

Doxaran, D., Froidefond, J.M., Lavender, S., & Castaing, P.: Spectral signature of highly turbid waters Application with SPOT data to quantify suspended particulate matter concentrations. Remote Sensing of Environment, 81, 149-161, doi.org/10.1016/S0034-4257(01)00341-8, 2002.

Feng, L., Hu, C., Chen, X., & Song, Q.: Influence of the Three Gorges Dam on total suspended matters in the Yangtze Estuary and its adjacent coastal waters: Observations from MODIS. Remote Sensing of Environment, 140, 779–788, doi.org/10.1016/j.rse.2013.10.002, 2014.

Feng, M., Sexton, J.O., Huang, C., Masek, J.G., Vermote, E.F., Gao, F., Narasimhan, R., Channan, S., Wolfe, R.E., & Townshend, J.R.: Global surface reflectance products from Landsat: Assessment using coincident MODIS observations.

Remote Sensing of Environment, 134, 276-293, 2013.

FRASER, R.N.: Multispectral remote sensing of turbidity among Nebraska Sand Hills lakes. International Journal of Remote Sensing, 19, 3011-3016, doi.org/10.1016/j.rse.2013.02.031, 1998.

Giardino, C., Brando, V.E., Dekker, A.G., Strömbeck, N., & Candiani, G.: Assessment of water quality in Lake Garda (Italy) using Hyperion. Remote Sensing of Environment, 109, 183–195, doi:10.1016/j.rse.2006.12.017, 2007.

Giardino, C., Bresciani, M., Valentini, E., Gasperini, L., Bolpagni, R., & Brando, V.E.: Airborne hyperspectral data to assess suspended particulate matter and aquatic vegetation in a shallow and turbid lake. Remote Sensing of Environment, 157, 48–57, doi.org/10.1016/j.rse.2014.04.034, 2015.

Gordon, H.R., & Wang, M.: Retrieval of water-leaving radiance and aerosol optical thickness over the oceans with SeaWiFS: a preliminary algorithm. Applied Optics, 33, 443-452, doi.org/10.1364/AO.33.000443, 1994.

HEDLEY, J.D., HARBORNE, A.R., MUMBY, P.J.: Simple and robust removal of sun glint for mapping shallow-water benthos. International Journal of Remote Sensing, 26(10), 2107-2112, DOI: 10.1080/01431160500034086, 2005.

Hochberg, E.J., Andréfouët, S., Tyler, M.R.: Sea surface correction of high spatial resolution IKONOS images to improve bottom mapping in near-shore environments. IEEE Transactions on Geoscience and Remote Sensing, 41(7), 1724-1729, DOI: 10.1109/TGRS.2003.815408, 2003.

Hsu, S.-C., & Lin, F.J.: Elemental characteristics of surface suspended particulates off the Changjiang estuary during the 1998 flood. Journal of Marine Systems, 81, 323–334, doi:10.1016/j.jmarsys.2010.03.001, 2010.

Hu, C., Chen, Z., Clayton, T.D., Swarzenski, P., Brock, J.C., & Muller-Karger, F.E.: Assessment of estuarine water-quality indicators using MODIS medium-resolution bands: Initial results from Tampa Bay, FL. Remote Sensing of Environment, 93, 423-441, DOI: 10.1016/j.rse.2004.08.007, 2004.

Huang, W., Mukherjee, D., & Chen, S.: Assessment of Hurricane Ivan Effects on Chlorophyll-a in Pensacola Bay by MODIS 250m Remote Sensing. Marine Pollution Bulletin, 62, 490-498, doi:10.1016/j.marpolbul.2010.12.010, 2011.

Islam, M.R., Yamaguchi, Y., & Ogawa, K.: Suspended sediment in the Ganges and Brahmaputra Rivers in Bangladesh: observation from TM and AVHRR data. HYDROLOGICAL PROCESSES, 15, 493–509, DOI: 10.1002/hyp.165, 2001.

Jiang, H., Feng, M., Zhu, Y., Lu, N., Huang, J., & Xiao, T.: An Automated Method for Extracting Rivers and Lakes from Landsat Imagery. Remote Sensing, 6, 5067-5089, doi: 10.3390/rs6065067, 2014.

Ju, J., Roy, D.P., Vermote, E., Masek, J., & Kovalskyy, V.: Continental-scale validation of MODIS-based and LEDAPS Landsat ETM+ atmospheric correction methods. Remote Sensing of Environment, 122, 175-184, doi:10.1016/j.rse.2011.12.025, 2012.

Kaufman, Y.J., & Tanré, D.: Strategy for direct and indirect methods for correcting the aerosol effect on remote sensing: From AVHRR to EOS–MODIS. Remote Sensing of Environment, 55, 65-79, doi:10.1016/0034-4257(95)00193-X, 1996.

Keiner, L.E., & Yan, X.H.: A Neural Network Model for Estimating Sea Surface Chlorophyll and Sediments from Thematic Mapper Imagery. Remote Sensing of Environment, 66, 153–165, doi.org/10.1016/S0034-4257(98)00054-6, 1998.

LATHROP, R.G., LILLESAND, T.M., & YANDELL, B.S.: Testing the utility of simple multi-date Thematic Mapper calibration algorithms for monitoring turbid inland waters. International Journal of Remote Sensing, 12(10), 2045-2063, doi.org/10.1080/01431169108955235, 1991.

Li, J., Shu, G., & Yaping, W.: Delineating suspended sediment concentration patterns in surface waters of the Changjiang Estuary by remote sensing analysis. Acta Oceanologica Sinica, 29, 38-47, DOI: 10.1007/s13131-010-0054-7, 2010.

Liu, Y., Islam, M.A., & Gao, J.: Quantification of shallow water quality parameters by means of remote sensing. Progress in Physical Geography, 27, 24-43, DOI: 10.1191/0309133303pp357ra, 2003.

Lu, C., Lv, H., & Li, Y.: Backscattering properties and parametric model of Taihu Lake based on spectral classification. Journal of Remote Sensing, 16, 417-434, 2012.

Ma, D., & Wang, J.: Evaluation on potential ecological risk of sediment pollution in main estuaries of China. China Environmental Science, 23, 521-525, 2003.

Ma, R., Duan, H., Tang, J., & Chen, Z.: Remote sensing of lake water environment. Beijing: Science Press, 2010.

Ma, R., Tang, J., Duan, H., & Pan, D.: Progress in lake water color remote sensing. Journal of Lake Sciences, 21, 143-158, DOI: 10.18307/2009.0201, 2009.

Maiersperger, T.K., Scaramuzza, P.L., Leigh, L., Shrestha, S., Gallo, K.P., Jenkerson, C.B., & Dwyer, J.L.: Characterizing LEDAPS surface reflectance products by comparisons with AERONET, field spectrometer, and MODIS data. Remote Sensing of Environment, 136, 1-13, doi.org/10.1016/j.rse.2013.04.007, 2013.

Masek, J.G., Vermote, E.F., Saleous, N.E., Wolfe, R., Hall, F.G., Huemmrich, K.F., Gao, F., Kutler, J., & Lim, T.-K.: A Landsat Surface Reflectance Dataset for North America, 1990–2000. IEEE GEOSCIENCE AND REMOTE SENSING LETTERS, 3, 68-72, doi:10.1109/LGRS.2005.857030, 2006.

May, C.L., Koseff, J.R., Lucas, L.V., Cloern, J.E., & Schoellhamer, D.H.: Effects of spatial and temporal variability of turbidity on phytoplankton blooms. MARINE ECOLOGY PROGRESS SERIES, 254, 111-128, DOI: 10.3354/meps254111, 2003.

Mei, A., Peng, W., Qin, Q., & Liu, H.: Introduction to Remote Sensing. Beijing: Higher Eduction Press, 2001.

Montanher, O.C., Novo, E.M.L.M., Barbosa, C.C.F., Renno, C.D., Silva, T.S.F.: Empirical models for estimating the suspended sediment concentration in Amazonian white water rivers using Landsat/TM. International Journal of Applied Earth Observation and Geoinformation, 29, 67-77, doi.org/10.1016/j.jag.2014.01.001, 2014.

Nas, B., Ekercin, S., Karabörk, H., Berktay, A., & Mulla, D.J.: An Application of Landsat-5TM Image Data for Water Quality Mapping in Lake Beysehir, Turkey. Water Air Soil Pollut, 212, 183-197, DOI: 10.1007/s11270-010-0331-2, 2010.

Nechad, B., Ruddick, K., & Park, Y.: Calibration and validation of a generic multisensor algorithm for mapping of total suspended matter in turbid waters. Remote Sensing of Environment, 114, 854–866, doi:10.1016/j.rse.2009.11.022, 2010.

Olmanson, L.G., Brezonik, P.L., & Bauer, M.E.: Airborne hyperspectral remote sensing to assess spatial distribution of water quality characteristics in large rivers-The Mississippi River and its tributaries in Minnesota. Remote Sensing of Environment, 130, 254–265, doi.org/10.1016/j.rse.2012.11.023, 2013.

Oyama, Y., Matsushita, B., Fukushima, T., Matsushige, K., & Imai, A.: Application of spectral decomposition algorithm for mapping water quality in a turbid lake (Lake Kasumigaura, Japan) from Landsat TM data. ISPRS Journal of Photogrammetry and Remote Sensing, 64, 73-85, doi:10.1016/j.isprsjprs.2008.04.005, 2009.

Pozdnyakov, D., Shuchman, R., Korosov, A., & Hatt, C.: Operational algorithm for the retrieval of water quality in the Great Lakes. Remote Sensing of Environment, 97, 352-370, doi:10.1016/j.rse.2005.04.018, 2005.

Raharimahefa, T., & Kusky, T.M.: Environmental Monitoring of Bombetoka Bay and the Betsiboka Estuary, Madagascar, Using Multi-temporal Satellite Data. Journal of Earth Science, 21, 210-226, DOI: 10.1007/s12583-010-0019-y, 2010.

Rao, K.H.V.D., Singh, A.K., & Roy, P.S.: Study of Morphology and Suspended Sediment of Bhopal Upper Lake using Spatial Simulation Technique and Remote Sensing Data. Indian Society of Remote Sensing, 37, 433–441, DOI: 10.1007/s12524-009-0034-6, 2009.

Ritchie, J.C., & Cooper, C.M.: An algorithm for estimating surface suspended sediment concentrations with Landsat MSS digital data. WATER RESOURCES BULLETIN, 27, 373-379, DOI: 10.1111/j.1752-1688.1991.tb01436.x, 1991.

Ritchie, J. C., & Zimba, P. V.: In M. G. Anderson (Ed.), 62: Estimation of Suspended Sediment and Algae in Water Bodies, DOI: 10.1002/0470848944.hsa066, 2005.

Shen, F., SALAMA, M.S., ZHOU, Y.-X., LI, J.-F., SU, Z., & KUANG, D.-B.: Remote-sensing reflectance characteristics of highly turbid estuarine waters – a comparative experiment of the Yangtze River and the Yellow River. International Journal of Remote Sensing, 31, 2639–2654, DOI: 10.1080/01431160903085610, 2010.

Shen, Z., Zhou, S., & Pei, S.: Transfer and transport of phosphorus and silica in the turbidity maximum zone of the Changjiang estuary. Estuarine, Coastal and Shelf Science, 78, 481-492, doi:10.1016/j.ecss.2008.01.010, 2008.

Sipelgas, L., Ossipova, V., Raudsepp, U., & Lindfors, A.: A bio-optical model for the calculation of suspended matter concentration form MODIS data in Pakri Bay, the gulf of Finland. BOREAL ENVIRONMENT RESEARCH, 14, 415-426, 2009.

Song, K., Wang, Z., Blackwell, J., Zhang, B., Li, F., Zhang, Y., & Jiang, G.: Water quality monitoring using Landsat Themate Mapper data with empirical algorithms in Chagan Lake, China. Journal of Applied Remote Sensing, 5, 053506-053516, doi: 10.1117/1.3559497, 2011.

Tang, J., Tian, G., Wang, X., Wang, X., & Song, Q.: The Methods of Water Spectra Measurement and Analysis: Above-Water Method. Journal of Remote Sensing, 8, 37-44, 2004a.

Tang, J., Wang, X., Song, Q., Li, T., Chen, J., Huang, H., & Ren, J.: The statistic inversion algorithms of water constituents for the Huanghai Sea and the East China Sea. Acta Oceanologica Sinica, 23, 617-626, 2004b.

Tang, W., Ma, C., Niu, S., Wang, X., Song, Q., & Ding, J.: Quantitative inversion of the water body composition based on CBERS02 datas. Science China E Information Sciences, 35, 156-170, 2005.

Topliss, B.J., Almos, C.L., & Hill, P.R.: Algorithms for remote sensing of high concentration, inorganic suspended sediment. International Journal of Remote Sensing, 11, 947-966, doi.org/10.1080/01431169008955069, 1990.

Vermote, E.F., Tanré, D., Deuzé, J.L., Herman, M., & Morcrette, J.-J.: Second Simulation of the Satellite Signal in the Solar Spectrum, 6S: An Overview. IEEE TRANSACTIONS ON GEOSCIENCE AND REMOTE SENSING, 35, 675-686, DOI: 10.1109/36.581987, 1997.

Vidot, J., & Santer, R.: Atmospheric correction for inland waters-application to SeaWiFS. International Journal of Remote Sensing, 26, 3663-3682, DOI: 10.1080/01431160500034029, 2005.

Volpe, V., Silvestri, S., & Marani, M.: Remote sensing retrieval of suspended sediment concentration in shallow waters. Remote Sensing of Environment, 115, 44-54, DOI: 10.1016/j.rse.2010.07.013, 2011.

Wang, C., Li, D., Wang, D., Chen, S., & Liu, W.: A total suspended sediment retrieval model for multiple estuaries and coasts by Landsat imageries. 2016 4th International Workshop on Earth Observation and Remote Sensing Applications, DOI: 10.1109/EORSA.2016.7552785, 2016.

Wang, H., Hladik, C.M., Huang, W., Milla, K., Edmiston, L., Harwell, M.A., & Schalles, J.F.: Detecting the spatial and temporal variability of chlorophylla concentration and total suspended solids in Apalachicola Bay, Florida using MODIS imagery. International Journal of Remote Sensing, 31, 439-453, DOI: 10.1080/01431160902893485, 2010.

Wang, L., Zhao, H., Song, C., Yuan, J., & Yu, H.: Coastal geomorphic evolut ion at the Denglou Cape, the Leizhou Peninsula. Acta Oceanologica Sinica, 21, 597-611, 2002.

Wu, G., Cui, L., Duan, H., Fei, T., & Liu, Y.: An approach for developing Landsat-5 TM-based retrieval models of suspended particulate matter concentration with the assistance of MODIS. ISPRS Journal of Photogrammetry and Remote Sensing, 85, 84–92, doi.org/10.1016/j.isprsjprs.2013.08.009, 2013.

Zhang, M., Dong, Q., Cui, T., Xue, C., & Zhang, S.: Suspended sediment monitoring and assessment for Yellow River estuary from Landsat TM and ETM+ imagery. Remote Sensing of Environment, 146, 136–147, doi.org/10.1016/j.rse.2013.09.033, 2014.

Zhang, Y., Zhang, B., Wang, X., Li, J., Feng, S., Zhao, Q., Liu, M., & Qin, B.: A study of absorption characteristics of chromophoric dissolved organic matter and particles in Lake Taihu, China. Hydrobiologia, 592, 105–120, DOI: 10.1007/s10750-007-0724-4, 2007.

Zhang, Y., Zhang, Y., Zha, Y., Shi, K., Zhou, Y., & Wang, M.: Remote Sensing Estimation of Total Suspended Matter Concentration in Xin'anjiang Reservoir Using Landsat 8 Data. Environmental Science, 36, 56-63, DOI: 10.13227/j.hjkx.2015.01.008, 2015.

Zhao, H., Chen, Q., Walker, N.D., Zheng, Q., & Macintyre, H.L.: A study of sediment transport in a shallow estuary using MODIS imagery and particle tracking simulation. International Journal of Remote Sensing, 32, 6653-6671, DOI: 10.1080/01431161.2010.512938, 2011.

Tables

Table 1. Information about the study areas and in-situ data

Location	Hydrologic features (Length, drainage area, mean surface runoff and sediment discharge)	Date	Samples	Measurements	Number of synchronous samples with satellite
Region I	—, — $8.6 \bullet 10^8 m^3$/year, $3 \bullet 10^4$ ton/year	Dec 3, 2010	10	Reflectance, TSS	No
		Jan 13~14, 2013	22	Reflectance, TSS	No
Region II	199 km, $6 \bullet 10^3$ km^2, $8.21 \bullet 10^9$ m^3/year, $3.27 \bullet 10^5$ ton/year	Dec 6, 2013	11	Reflectance, TSS	7, OLI
Region III	2320 km, $4.53 \bullet 10^5$ km^2, $3.26 \bullet 10^{11}$ m^3/year, $7.53 \bullet 10^7$ ton/year	Dec 19, 2006	5	Reflectance, TSS	No
		Dec 21, 2006	18	8 samples with Reflectance and TSS; 10 samples with TSS only	13, Hyperion
		Dec 27, 2007	8	Reflectance, TSS	No
		Nov 2, 2012	9	Reflectance, TSS	6, ETM+
Region IV	470 km, $3.01 \bullet 10^4$ km^2, $2.45 \bullet 10^{10}$ m^3/year, $6.93 \bullet 10^6$ ton/year	Dec 1, 2013	12	Reflectance, TSS	9, OLI
Region V	6280 km, $1.8 \bullet 10^6$ km^2, $9.2 \bullet 10^{11}$ m^3/year, $4.8 \bullet 10^8$ ton/year	Oct 14~15, 2009	34	Reflectance, TSS	No

Table 2. Review of previous TSS or Turbidity retrieval models using Landsat imagery.

Data	Model	Study area	Reference
TM Bands 2, 4	TSS=29.022•exp(0.0335•(B4/B2))	Gironde and Loire Estuaries	Doxaran et al. (2003)
MSS Bands 5, 6	Ln(TSS)= 1.4•(B5/B6)^2-6.2•(B5/B6) +10.8	the Bay of Fundy and the Beaufort Sea	Topliss et al. (1990)
TM Bands 1, 3, 4	Turbidity=11.31•(B4/B1)-2.03•B3-16.42	Chagan Lake	Song et al. (2011)
TM Band 4	Turbidity=16.1•B4-12.7	Nebraska Sand Hills Lakes	Fraser. (1998)
TM Band 3	Turbidity=10•B3-24.8		
TM Band 1	Turbidity=19•B1-97.9		
TM Band 2	Turbidity=6.4•B2-28		
TM Band 3	TSS=69.39•B3-201	Ganges and Brahmaputra Rivers	Islam et al. (2001)
MSS Bands 1, 2	Ln(TSS)= 2.71•(B1/B2)^2-9.21•(B1/B2) +8.45	Enid Reservoir in North Central Mississippi	Ritchie and Cooper. (1991)
TM Band 3	Log(TSS)= 0.098•B3+0.334	Delaware Bay	Keiner and Yan. (1998)
TM Bands 2, 3	TSS=0.7581•exp(61.683•(B2+B3)/2)	southern Frisian lakes	Dekkera et al. (2001)
TM Bands 1, 3	TSS=0.0167•exp(12.3•B3/B1)	an embayment of Lake Michigan	Lathrop et al. (1991)
TM/ETM+ Band 3	Log(TSS)= 44.072•B3 +0.1591	Yellow River estuary	Zhang et al. (2014)
TM Band 3	TSS=2.19•exp(21.965•B3)	Poyang Lake	Wu et al. (2013)
	TSS=-9275.78•(B3)^3+8623.19•(B3)^2		

	-810.04•B3+23.44		
TM Bands 3, 4	TSS=5829.8•(B3-B4)^3+4165.09•(B3-B4)^2 -189.88•(B3-B4)+5.43		
	TSS=3.411•exp(21.998•(B3-B4))		
OLI Bands 2, 3, 8	TSS=-191.02•B2+36.8•B3+172.66•B8+4.57	Xin'anjiang Reservoir	Zhang et al. (2015)
TM Band 2	B2=0.0044•TSS+2.5226	Bhopal Upper Lake	Rao et al. (2009)
TM Band 2, 3	Log(TSS)= 6.2244•(B2+B3)/B2•B3+0.892	Yangtze estuary	Li et al. (2010)
TM Band 3	TSS=0.543•B3-7.102	Beysehir Lake	Nas et al. (2010)
TM Band 4	TSS=229457.695•(B4)^2+146.462•B4+5.701	Bohai gulf	Chen et al. (2014)

Table 3. The comparison of calibration and validation accuracy of several best TSS retrieval models

Model form		Calibration (R^2)	Validation (RMSE(mg/L), MRE)		
			Whole	Low range	High range
Chen et al. (2014)		0.7842	35.7, 144.2%	18.35, 215.58%	53.56, 23.5%
Li et al. (2010)		0.6167	69.3, 45%	5.66, 52.6%	113.48, 32.1%
Zhang et al. (2014)		0.5804	82.8, 48%	6.56, 53.9%	135.54, 38.15%
Lathrop et al. (1991)		0.6661	50.3 39.4%	6.12, 44.6%	82.09, 30.57%
Ritchie and Cooper. (1991)		0.6983	68.7, 41.3%	7.24, 44%	112.32, 36.6%
This study	OLI	0.7181	21.5, 27.2%	3.5, 31.1%	35.1, 20.7%
	ETM+	0.708	25, 32.5%	4.6, 38.3%	40.7, 20.3%
	TM	0.7079	24.9, 31.5%	4, 35.3%	40.6, 25.1%

Table 4. The performance of different sensors and the vertexs of QRLTSS model based on these sensors

	TM	ETM+	OLI	MODIS
	Red band, Near infrared band	Red band, Near infrared band	Red band, Near infrared band	Red band, Near infrared band
Wavelength (nm)	630-690, 760-900	630-690, 775-900	630-680, 845-885	620-670, 841-874
Spatial resolution (m)	30	30	30	250
Radiometric resolution (bit)	8	8	12	12
Signal/noise (dB and Specified level of high)	140, 244	140, 244	340, 460	128, 201
The vertex of quadratic model	0.031, 32.2 mg/L (This study)	0.031, 32.2 mg/L (This study)	0.032, 36.1 mg/L (This study)	0.025, 31 mg/L (Chen et al., 2015b)

Figures

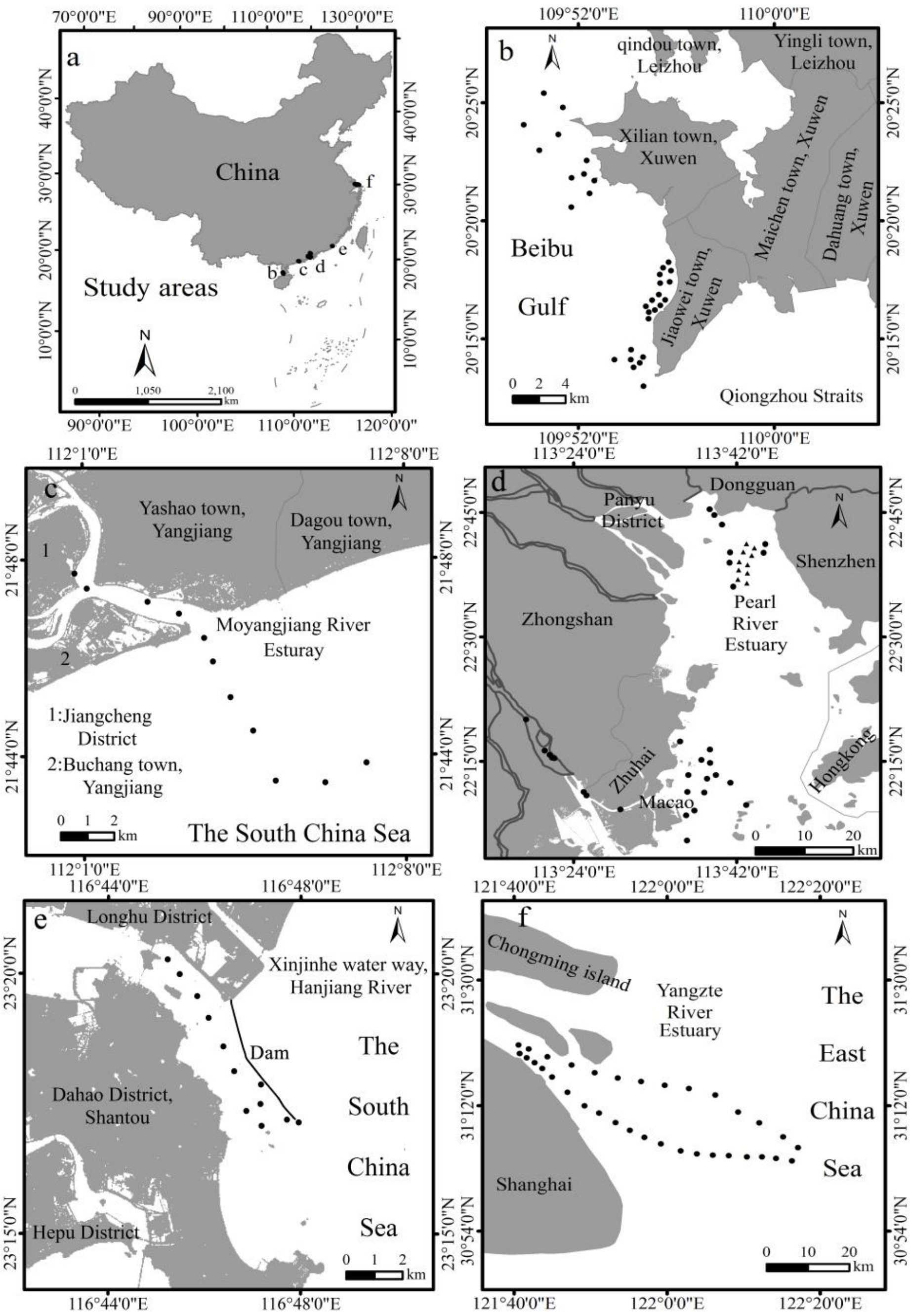

Figure 1. Study areas and locations of in situ data (black dots and triangles). b: Xuwen coast; c: Moyangjiang River Estuary; d: Pearl River Estuary; e: Hanjiang River Estuary; f: Yangtze River Estuary.

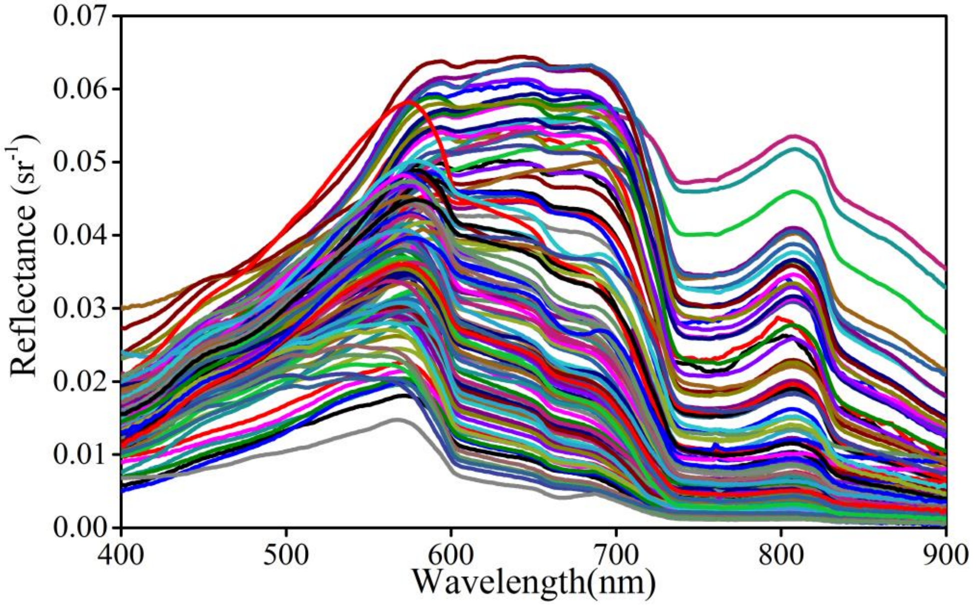

Figure 2. 119 spectra were collected from study areas by ASD

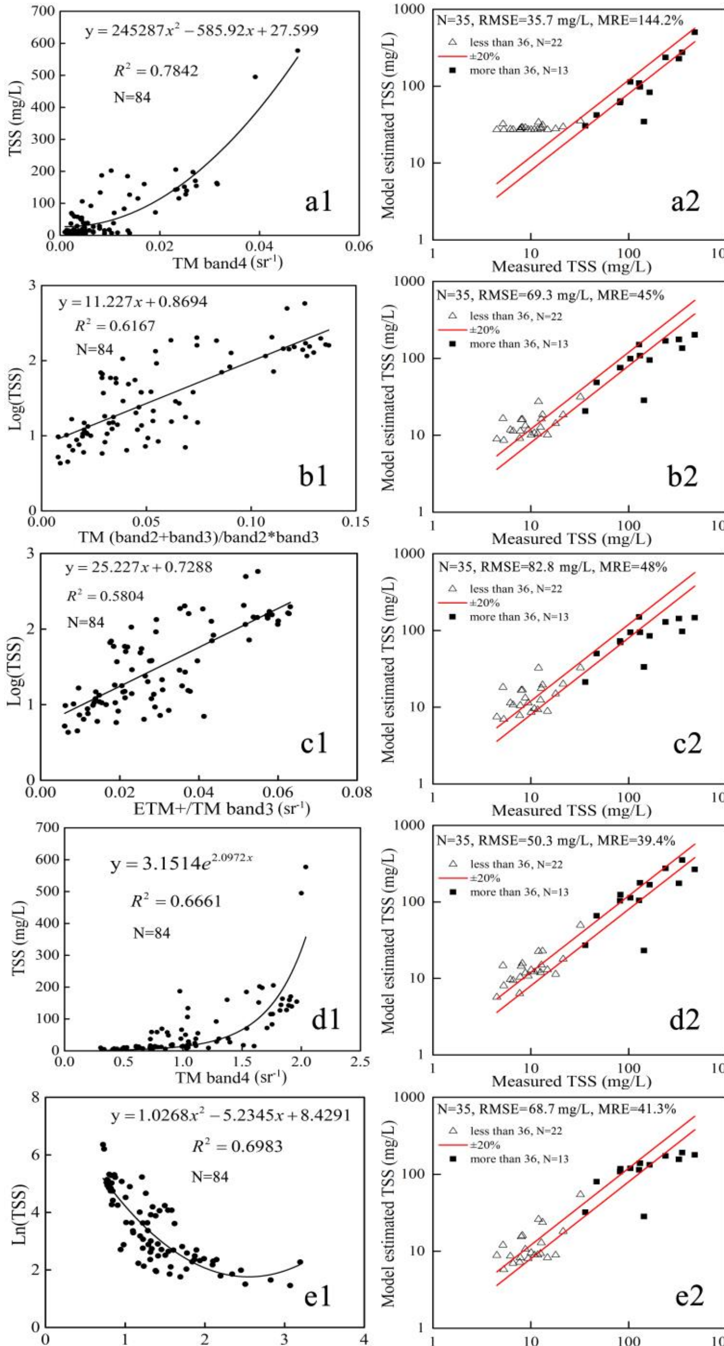

Figure 3. The recalibration and validation of previous five TSS retrieval models based on 119 in situ samples. The models were developed by a (Chen et al., 2014), b (Li et al., 2010), c (Zhang et al., 2014), d (Lathrop et al., 1991), e (Ritchie and Cooper., 1991), respectively.

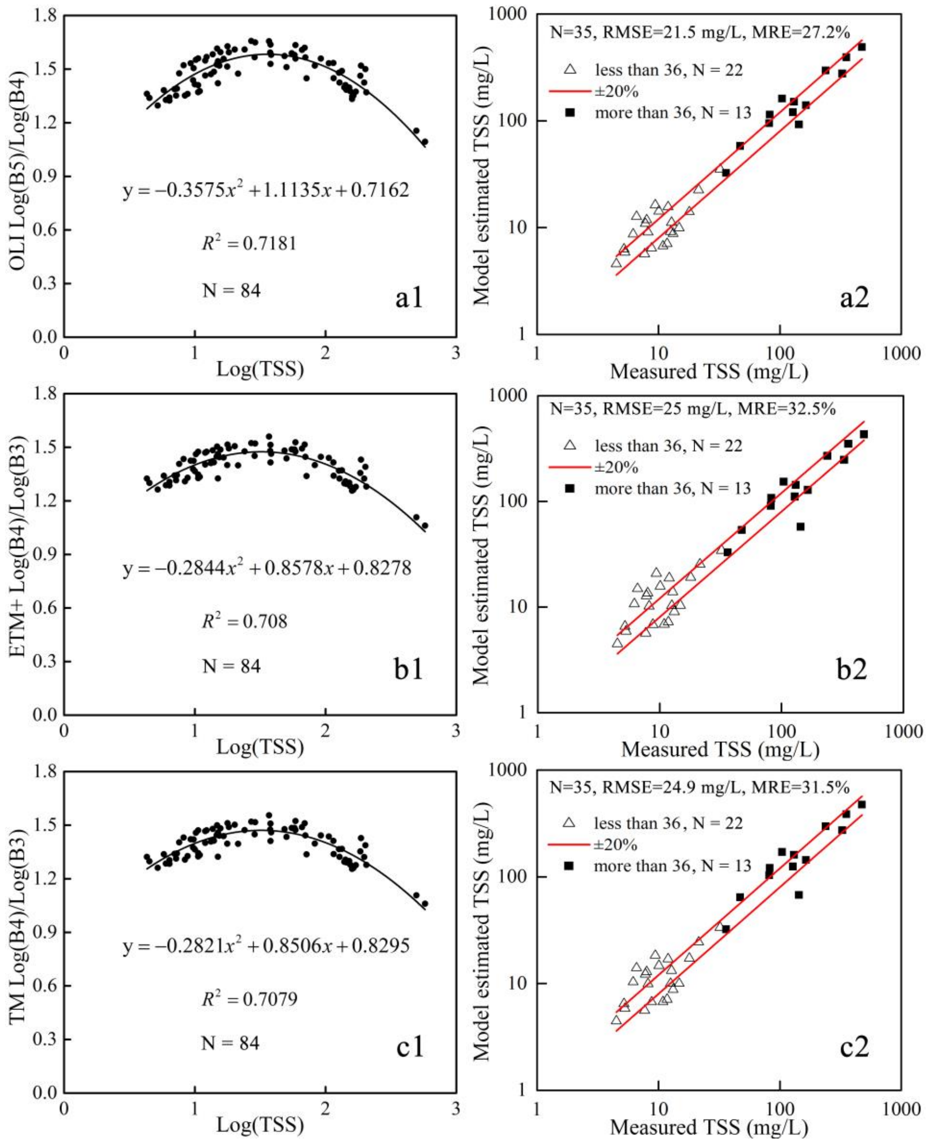

Figure 4. The calibration and validation results of TSS retrieval models: based on 119 in situ data (a) OLI, (b) ETM+ and (c) TM.

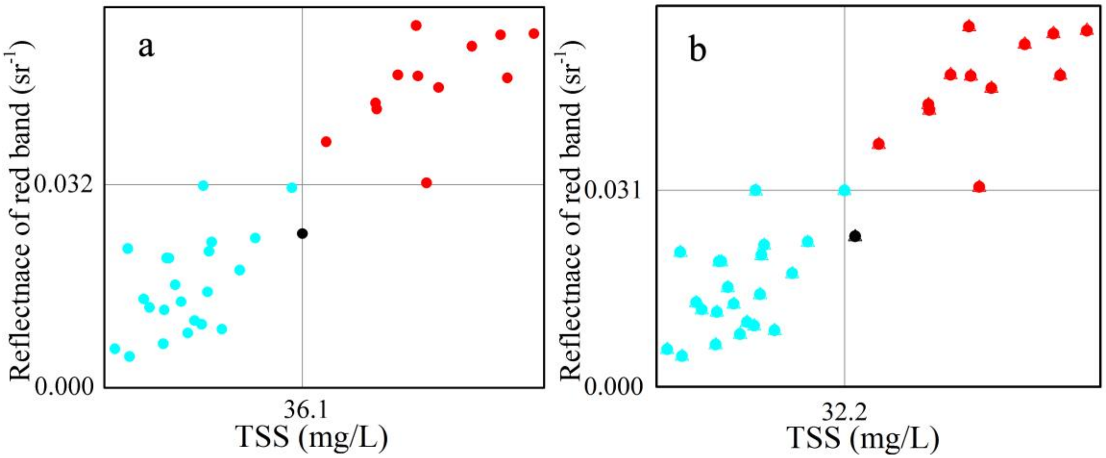

Figure 5. Relationship between the Landsat red band reflectance and corresponding TSS concentration. a: OLI sensor; b: ETM+ and TM sensors.

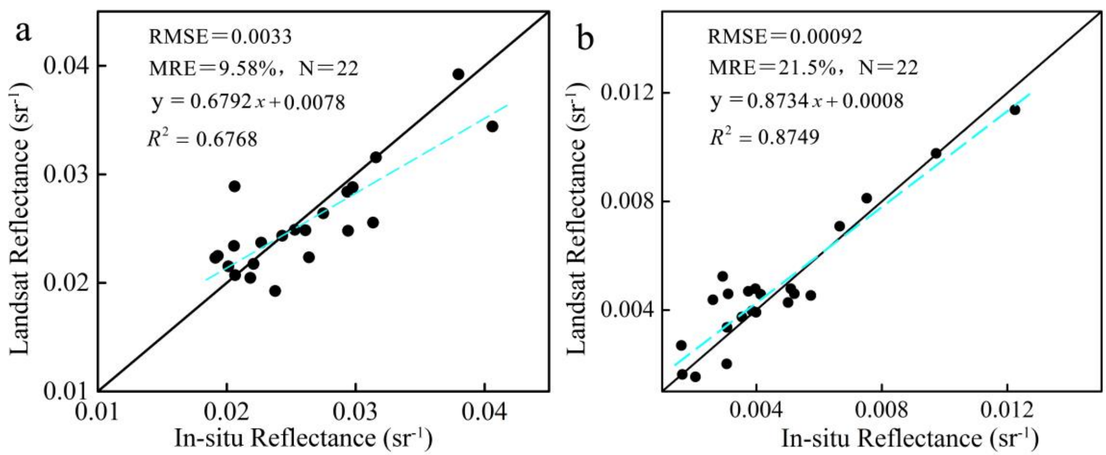

Figure 6. Scatterplot of Landsat measured reflectance versus in-situ reflectance. The former is calculated by averaging over a box of 3x3 pixels centered samples. a: red band; b: near infrared band.

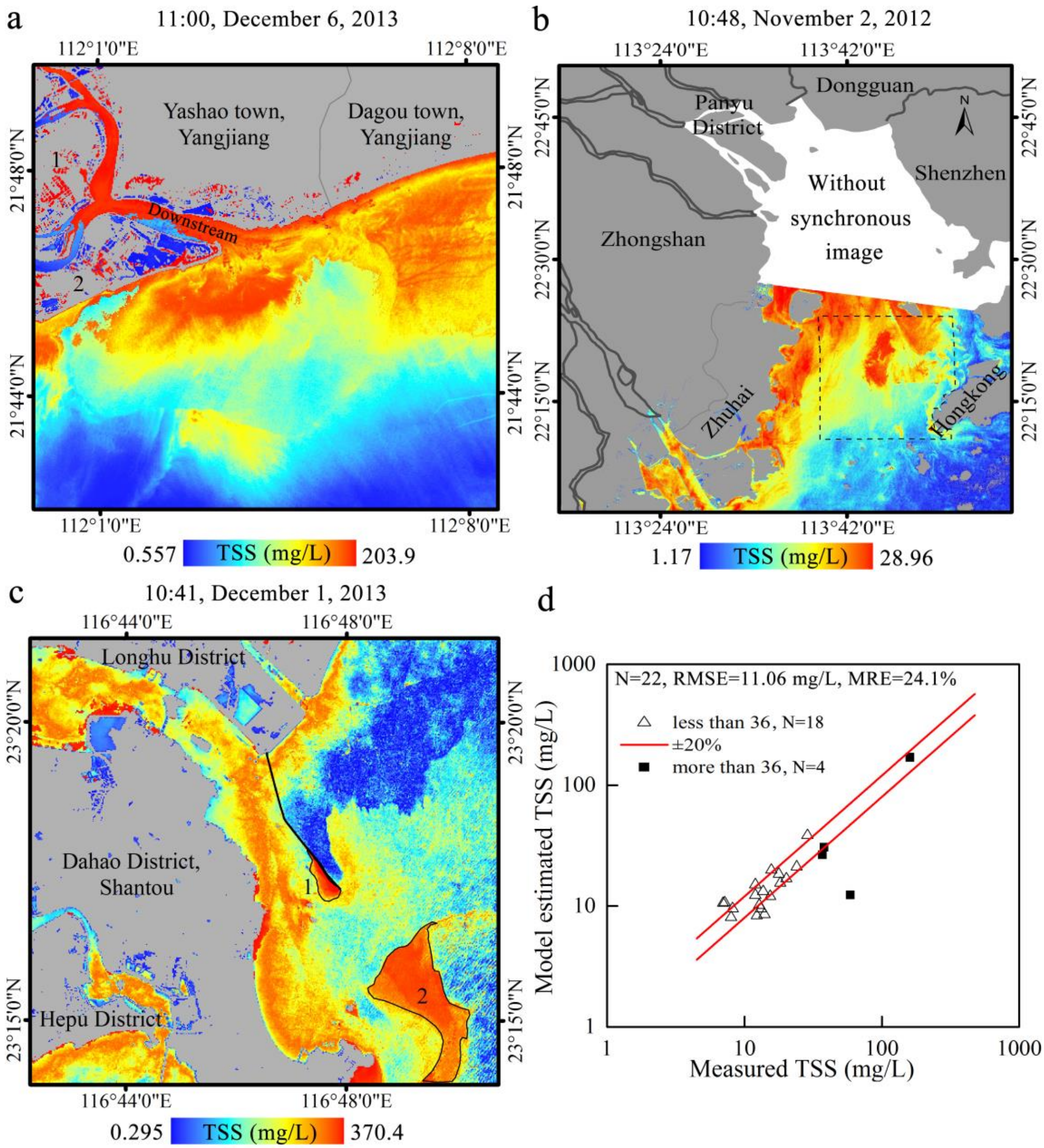

Figure 7. Estimated TSS concentrations based on QRLTSS model in Moyangjiang River Estuary at 11:00 (Beijing time, OLI), on December 6, 2013 (a), Pearl River Estuary at 10:48 (Beijing time, ETM+), on November 2, 2012 (b), Hanjiang River Estuary at 10:41 (Beijing time, OLI), on December 1, 2013 (c), and comparison between the in-situ measured and Landsat imagery inversed TSS concentrations of three estuaries (d). Color scale is the legend of the TSS concentrations, in mg/L.

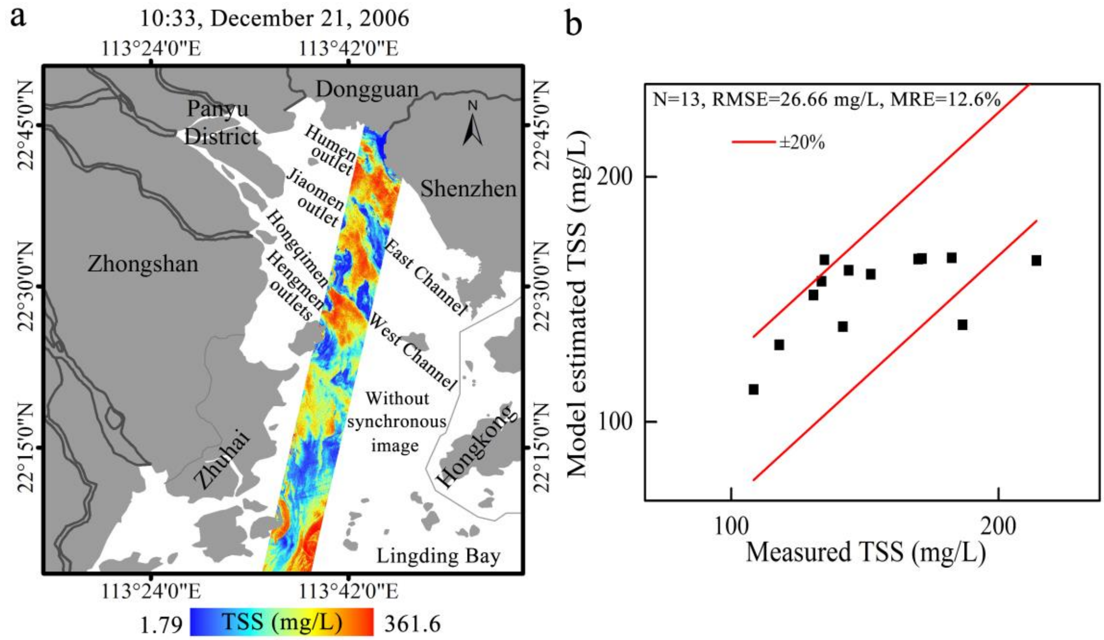

Figure 8. Estimated TSS concentrations based on QRLTSS model from EO-1 Hyperion imagery in Pearl River Estuary at 10:33 (Beijing time), on December 21, 2006 (a) and comparison between the in-situ measured and EO-1 Hyperion imagery inversed TSS concentrations (b). Color scale is the legend of the TSS concentrations, in mg/L.